

Axon targeting of transcriptionally distinct pioneer neurons is regulated by retinoic acid signaling

Received: 9 July 2024

Accepted: 11 June 2025

Published online: 01 July 2025

Benjamin M. Woodruff¹, Lauren N. Miller¹, Nicholas L. Calistri²,
Jacqueline R. McVay¹, Laura M. Heiser² & Alex V. Nechiporuk¹✉

During nervous system development, pioneer neurons (pioneers) extend their axons toward distant targets, creating a scaffold for follower neurons and defining the initial structure of the nervous system. Despite years of study, whether pioneer neurons are transcriptionally distinct from followers is unknown. To address this question, we performed single-cell RNA sequencing (scRNA-seq) of zebrafish posterior lateral line (pLL) sensory neurons and found that pioneers and followers are transcriptionally distinct populations. Interestingly, expression profiling of differentiating pLL progenitors defines “follower” as the ground state and “pioneer” as a later developmental state, with retinoic acid (RA) signaling active in all pLL progenitors. Modulation of RA signaling within single pLL neurons demonstrated that its downregulation is necessary for expression of a neurotrophic factor receptor *ret*, which is required for correct targeting of pioneer axons. Our study reveals molecular heterogeneity between pioneers and followers and implicates RA signaling in fidelity of pioneer axonal targeting.

The nervous system is an extensive and complex network of neural connections, many of which are established during embryonic development. Pioneer neurons (hereafter, pioneers) exhibit the remarkable ability to navigate through developing tissue and build the initial scaffold of the nervous system^{1,2}. Pioneers were first discovered about 50 years ago as a class of neurons that extend their axons into non-innervated tissue, enabling the subsequent recruitment of additional, follower axons¹. This contrasts with follower neurons which will extend later along the trail laid down by pioneers to connect to their targets. In many systems, followers exhibit difficulty navigating to appropriate targets when pioneers are ablated^{3–8}.

When compared to followers in certain contexts, pioneers have larger cell bodies, more elaborate growth cones, different axon growth rates, and can undergo more complex pathfinding^{9–13}. This definition has endured to the present day as pioneers are still largely described by morphology and behavior^{14,15}. However, recent evidence from our work, and from others', shows at least some

molecular differences between pioneers and followers in multiple systems. For example, in *C. elegans*, pioneer and follower neurons are guided by glial cells using distinct molecular cues¹⁶. Similarly, our previous work showed that the extension of pioneers, but not followers, in the peripheral sensory system of zebrafish is directed by a specific neurotrophic factor receptor, Ret⁵. Finally, manipulation of Jun kinase (JNK) activity in the *Drosophila* ventral nerve cord selectively affects pioneer, but not follower, neurons¹⁷. However, whether the above observations imply more profound molecular differences between pioneer and follower neurons in any system is not known.

To examine the behavior and molecular identity of pLL neurons during differentiation and axon outgrowth, we took advantage of the zebrafish posterior lateral line (pLL) as a model system^{5,18}. The pLL is a mechanosensory system in aquatic vertebrates that detects water movement and regulates swimming behaviors such as schooling, predator and prey detection, and maintenance of rheotaxis^{18–21}.

¹Department of Cell, Developmental & Cancer Biology, Oregon Health & Science University, Portland, Oregon, USA. ²Biomedical Engineering, Oregon Health & Science University, Portland, Oregon, USA. ✉ e-mail: nechipor@ohsu.edu

The pLL consists of sensory neurons that innervate mechanosensory organs called neuromasts (NMs) located on the surface of the trunk.

Both sensory and neural progenitors derive from the pLL placode, a thickening of the embryonic ectoderm, that forms shortly after the end of gastrulation (10–14 h post fertilization or hpf)²² (Fig. 1A). At 22 hpf, pLL neurons initiate axon extension caudally from a cranial ganglion (Fig. 1B). Between 3–6 pLL pioneer axon growth cones are embedded within the pLL primordium (pLLP), a group of sensory organ progenitors that migrates along the trunk from 22 to 48 hpf²³ (Fig. 1C). As the pLLP migrates, it deposits 5 to 6 cell clusters at regular intervals as well as a terminal cluster, which differentiate into 2 to 3 NMs^{24–26}. By the end of primordium migration, pioneer axons reach the end of the tail and selectively innervate distal NMs. (Fig. 1D). Follower axons begin extension after pioneers, co-fasciculate with pioneer axons, and selectively innervate proximal NMs^{11,12,24,27}. Besides distinct targets, pLL pioneers also have larger cell bodies and more elaborate axon growth cones than followers^{5,9,12}.

Components of the pLL are easily visualized by transgenic reporter lines such as TgBAC(*neurod1:EGFP*)^{nl} (referred to as *neurod1:egfp*) which labels neurons^{5,28}, and Tg(-8.0*cldnB:LY-EGFP*)^{zn06} (referred to as *cldnB:memgfp*)²⁹ which labels both pLL neurons and the pLLP. The ability to distinguish and visualize pioneer pLL neurons in a live animal makes this system uniquely suited for transcriptomic analysis and follow up studies to define the function of genes required for pioneer axon growth and function.

Previous studies have defined a developmental timeline of pLL neuron differentiation. At mid-somitogenesis (14 hpf), pLL progenitors begin to undergo neurogenesis, which can be detected by expression of proneural factors, *neurog1* and *neurod1*^{28,30}. By 18 hpf, the pLL placode separates into committed sensory and neural progenitors³¹. One of the signals required for the initial formation of the pLL placode is retinoic acid (RA)³². RA is a small lipophilic molecule that acts as a morphogen to regulate gene expression and cellular differentiation^{33–38}. Upon cellular uptake, RA is translocated to the nucleus where it binds nuclear receptors, RAR and RXR, to activate transcription^{39–41}. Some RA signaling pathway components are also crucial mediators of RA signaling. For example, cellular retinoic acid-binding protein 1b (Crabp1b) binds intracellular RA to modulate signal intensity^{42–44}. RA signaling is also a well-established direct regulator of *hox* gene family members, including *hoxb5a*^{45–49}. RA has been well studied in many systems, including neurodevelopment; however, whether the RA signaling network remains active through neurogenesis and differentiation in the pLL is not known.

In this study we investigated transcriptional differences between pioneer and follower neurons of the zebrafish pLL. Using single-cell RNA-sequencing (scRNA-seq), we found that pioneers exhibit a transcriptional profile distinct from followers, including differential expression of neurotrophin receptors and components of the RA pathway. Surprisingly, analysis of pioneer and follower gene expression during early stages of pLL differentiation revealed that the default state for pLL progenitors is the follower identity, whereas the pioneer state is acquired. Live imaging of individually labeled pioneer and follower neurons revealed distinct morphology, growth, and behavior: most pioneer neurons delaminate first from the pLL placode, become bipolar, and extend their axons prior to followers. Ablation of pLL pioneer neurons revealed that they are required for follower axon extension in the pLL, further underscoring their essential role in axon guidance. We also show that the RA pathway is initially active in all pLL progenitors and is subsequently downregulated specifically in pioneers. This, in turn, is required for the expression of neurotrophic factor receptor Ret, which directs targeting of pioneer axons to distal sensory organs. We propose that a unique molecular program underlies the distinctive behavioral characteristics of pioneer neurons.

Results

scRNA-seq identifies two distinct populations of neurons within the pLL

We previously showed that pLL pioneers, in addition to having distinct morphology and target innervation, are enriched with the neurotrophic factor receptor Ret⁵. Based on these observations, we hypothesized that pLL pioneers are transcriptionally distinct from followers. To test this, we characterized transcriptional profiles of pLL pioneers and followers during axon extension (30 hpf) using scRNA-seq.

To isolate pLL neurons, we FAC sorted cells from *neurod1:egfp* embryos (Fig. 1E), as this transgene marks both CNS and PNS neurons including the pLL²⁸. Fortunately, the transgene is expressed at higher levels in cranial ganglia at 30 hpf, including the pLL^{5,28}; thus, we FAC sorted the top 2% brightest EGFP-expressing cells. This approach yielded 9242 cells, most of which were neurons, as well as some *neurod1*-expressing pancreas cells⁵⁰ (Fig. 1F and Fig. S1B), represented in 30 clusters. Using known tissue-specific markers, we identified each cell population (Fig. S1A). We identified the pLL by expression of known LL markers, such as *ret*⁵, *stmn2a*⁵¹, *bmper*⁵², and *rspo2*⁵³ (Fig. 1G–J), and exclusion of markers of other cranial sensory populations, such as *irx1a*⁵⁴ (otic) and *phox2bb*⁵⁵ (epibranchial) (Fig. S1A), as well as anterior LL marker *alcama*⁵⁶.

We then performed unsupervised subclustering of pLL cells which yielded two distinct subpopulations (Fig. 1K), one of which was highly enriched for *ret* (Fig. 1L, P). Differential expression (DE) analysis with a minimum difference threshold set at 25% and false discovery rate of <5% yielded 101 DE genes: 60 enriched in *ret*⁺ cells, 41 in *ret*⁻ cells (Fig. S2; Supplementary Table 1). Some examples of genes with the highest log₂ fold change in either the *ret*⁺ or *ret*⁻ populations are *gfra1a*, *ntrk1*, and *rpz5*, or *ntrk3a*, *nr2f2*, and *zfhx3*, respectively. (Fig. 1L–O and Fig. S2). The DE genes included several neurotrophin receptors: *ret*, *gfra1a*, and *ntrk1* were upregulated in *ret*⁺ cells, whereas *ntrk3a* was upregulated in *ret*⁻ cells (Fig. 1P). In addition, we found that the RA pathway member *crabp1b* and known transcriptional targets of RA in other systems (*hoxb5a*, *nr2f2*, and *zfhx3*) were upregulated in the *ret*⁻ population^{44,45,57–60}. In summary, scRNA-seq identified two distinct populations within the developing pLL ganglion, delineated by their relative expression of the previously defined pLL pioneer marker *ret*. Together with our previous study, these data suggest that the *ret*⁺ cells are pioneers, whereas the *ret*⁻ cells are followers.

Pioneer and follower neurons are transcriptionally distinct

Next, we validated our sequencing data expression profiles. We performed whole-mount fluorescent in situ hybridization (FISH) using RNAscope[®]^{61,62}. We used the *cldnB:memgfp* transgenic as it labels cell membranes in the pLL ganglion^{29,63} which allows identification of individual neurons for signal quantification (Fig. 2A, B). We probed for genes differentially expressed in the *ret*⁺ and *ret*⁻ clusters in pairwise combinations (Fig. 2C–E). We found that genes in each cluster had high correlation coefficients amongst each other, indicating expression within the same neurons (Fig. 2F, G, and I, Fig. S3A, B). By contrast, comparing gene expression between *ret*⁺ and *ret*⁻ clusters displayed low correlation coefficients, (Fig. 2H, I, Fig. S3C, D), indicative of mutually exclusive expression. These data validate our scRNA-seq findings that *ret*⁺ and *ret*⁻ cells express distinct gene sets.

We then asked whether the *ret*⁺ cells are in fact pioneer neurons. To address this, we knocked in a red fluorescent protein, mRuby, into the *rpz5* locus using the mBait strategy⁶⁴. We chose *rpz5* because it is the most specific and highly enriched gene within the *ret*⁺ subpopulation (Fig. 1M, P). Validation of *rpz5:mRuby* expression by FISH with both *mRuby* and *rpz5* probes showed that 91% of mRuby⁺ cells (90/99) expressed the *rpz5* transcript (Fig. S4A, B), indicating that the transgene faithfully recapitulates endogenous expression of *rpz5*. As shown in Fig. 2J, mRuby marks a subset of pLL neurons during axon outgrowth

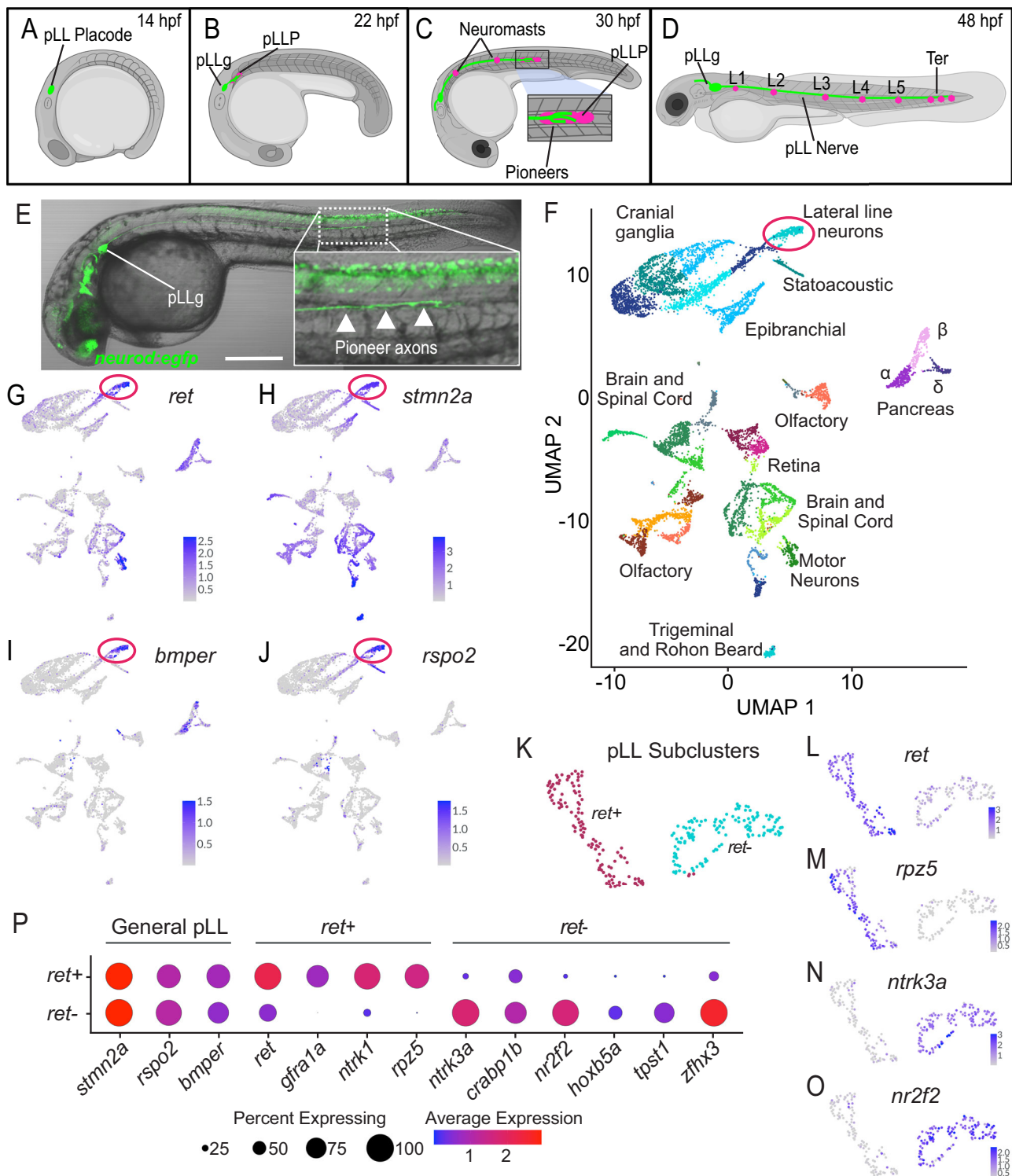
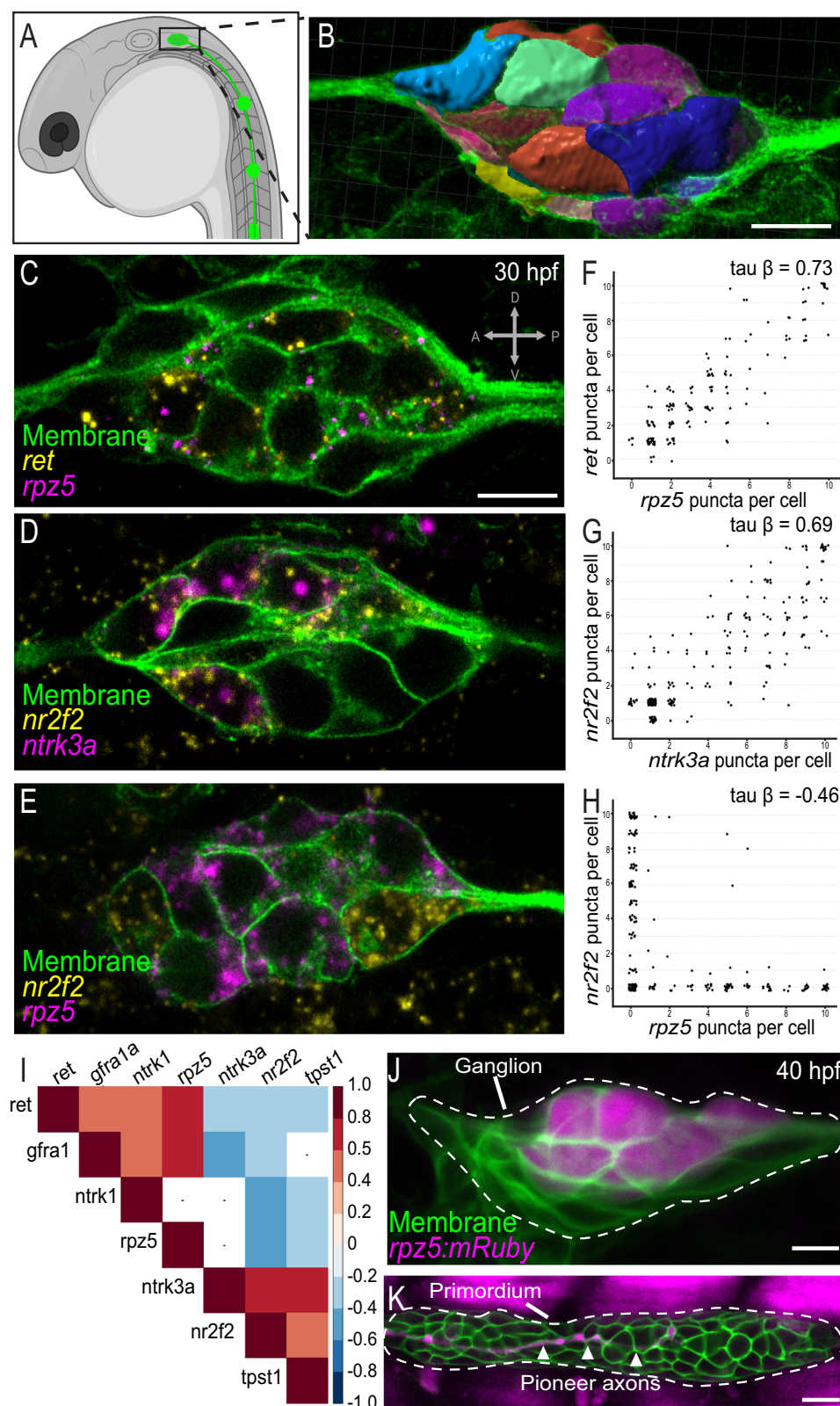


Fig. 1 | scRNA-sequencing identifies two transcriptionally distinct populations of pLL neurons. A–D Schematic of pLL development. **A** At 14 hpf, the posterior lateral line placode contains both neural and sensory progenitors. **B** At 22 hpf, the pLLP begins migrating and pioneer axons are already embedded within it. **C** At 30 hpf, the pLLP and pioneer axons reach halfway down the trunk. **D** At 48 hpf, the pLLP and lateral line pioneer axons have reached the end of tail. Abbreviations: pLLg – pLL ganglion; L1–L5 are lateral trunk NMs; Ter – terminal cluster of NMs. Created in BioRender. Lab, N. (2025) <https://BioRender.com/vij5z6b>. **E** *neurod1:egfp* transgene labels a subset of CNS and PNS neurons at 30 hpf, including the pLL^{5,28}.

White arrowheads mark extending pioneer axons in the inset. Scale bar = 200 μ m. **F** UMAP of all 30 hpf, EGFP+ sorted and sequenced cells. Major cell types are indicated. Red circle: lateral line neurons. **G–J** Feature plots showing expression of lateral line specific markers: *ret*, *stmn2a*, *bmper*, and *rspo2*. Red circle: lateral line neurons. **K** pLL subclusters: *ret+* and *ret-* populations. **L–O** Feature plots of subpopulations showing several differentially expressed genes in each subcluster. **P** Dotplot showing genes expressed in all pLL neurons as well differentially expressed genes in each subcluster.



(40 hpf). pLL neuron cell bodies that target distal neuromasts (i.e., pioneer neurons) localize dorsally in the pLLg after 30 hpf^{5,12}; we observed that mRuby⁺ cells occupied dorsal positions at 40 hpf. Importantly, mRuby consistently labeled the distal-most pioneer axons that migrate within the pLL during pLL nerve extension (Fig. 2K). We identified between three and seven mRuby⁺ cells within the ganglion (Fig. S4C). This is consistent with our previous observation demonstrating three to

six pioneer growth cones within the migrating pLLP⁵. In summary, our data demonstrate that pLL pioneer and follower neurons are transcriptionally distinct during axon extension.

pLL pioneer neurons are required for follower axons' extension

A typical behavioral characteristic of pioneer neurons is their ability to guide followers. To determine whether this mechanism is

Fig. 2 | Validation of scRNA-seq data identifies *ret*⁺ neurons as pioneers.

A Schematic of a 30 hpf embryo, a stage utilized for FISH. Membranes are labeled by *cldnB:memgfp* transgene (green). Created in BioRender. Lab, N. (2025) <https://BioRender.com/mdz3df6>. **B** 3D reconstruction of individual pLL neurons by Imaris using membrane-tagged *cldnB:memgfp* fluorescence. Subsequently, binned fluorescent puncta are counted in each individual cell. **C–E** Representative single Z-slice confocal images through the pLL ganglion showing pairwise FISH of two genes from *ret*⁺ and *ret*[−] subclusters (*ret* and *rpz5*, *nr2f2* and *rpz5*, or *nr2f2* and *ntrk3a*) at 30 hpf. Note that genes from the same clusters are coexpressed, whereas genes from the *ret*⁺ and *ret*[−] subclusters are largely expressed in different cells. **F–H** Quantification of gene expression shown in **C–E**. Each dot corresponds to a single cell and the axes indicate binned gene expression levels. Each plot shows all

cells across 10 embryos. Gene expression within the same pLL subcluster is strongly correlated, whereas gene expression between different pLL subclusters is not.

I Heatmap shows pairwise Kendall tau-beta gene correlation coefficients based on examining expression of gene pairs by FISH. Empty squares represent untested probe combinations. **J** Z-projection of *rpz5:mRuby* pLLg. Cell membranes are marked by *cldnB:memgfp* transgene. Note that only a subset of dorsal pLL neurons is mRuby-positive at 40 hpf ($n = 6$). **K** Confocal image of the migrating pLL primordium from the same animal shown in (**J**). Note the presence of mRuby-positive axons embedded within the primordium (dashed outline) indicating that labeled pLL cells are indeed pioneer neurons. mRuby labeling dorsal to pLL primordium is muscle. All scale bars = 10 μ m. All images scaled the same.

present in the pLL, we used a two-photon cell ablation strategy to selectively remove pioneer neurons⁶⁵. We utilized a transgenic line, TgBAC(*ret:EGFP*)^{b1331} (hereafter, *ret:egfp*), to visualize *ret*-expressing pLL neurons at the onset of axon extension⁶⁶ (Fig. 3A, B, Fig. S5A). At this stage, two to five pLL neurons begin expressing the transgene. In situ hybridization with the *ret* probe showed that the endogenous *ret* expression correlated relatively well with *ret:egfp* (65% of EGFP⁺ were also *ret*⁺), with the brightest EGFP⁺ cells being the strongest expressers of *ret* (Fig. S5B, C). We ablated EGFP⁺ neurons between 22 and 23 hpf and tracked axon extension using the *neurod1:mCherry* transgene for 5 to 10 h (Fig. 3A). In unablated controls, the pLL nerve migrated an average of 6.7 somites (Fig. 3B, C, Supplementary Movie 1; Table 1). In contrast, the ablation of *ret:egfp*⁺ neurons completely blocked pLL nerve extension. Interestingly, pLL axon terminals still displayed dynamic movements, but clearly lacked the ability to advance (Fig. 3D, E, Supplementary Movie 2; Table 1). When only a subset of *ret:egfp*⁺ neurons were ablated, the pLL nerve extended comparably to controls, indicating that the ablation procedure itself does not impair pLL nerve extension (Fig. 3F, G; Supplementary Movie 3). It also showed that as few as two pioneer axons are sufficient to support pLL nerve extension, a finding consistent with previous pioneer ablation studies⁶⁷. These experiments demonstrate that pLL pioneers are required for follower axon extension.

To identify potential pLL pioneer specific signals that guide followers, we used the CellChat package to search for transmembrane cell-to-cell communications networks⁶⁸. We used pLLP cells as a positive control (Fig. S6A), as several signaling networks between extending pLL neurons and pLLP, including Ret-Gdnf and Ntrk1-Ngf, have been previously defined^{69,70}. Indeed, both receptor-ligand pairs were identified by CellChat (Fig. S6A, B). Ncam, Cadm3, and teneurin-1 signaling had the highest communication probability of signaling between pioneers and followers (Fig. S6B–E). Notably, Cntn1b was the only pioneer-specific transmembrane molecule that had a follower specific partner (Fig. S6B–E). These findings highlight a set of candidate receptor-ligand interactions that may mediate pioneer-follower communication, with Cntn1b emerging as a uniquely pioneer-specific signal targeting followers.

Follower-specific markers define pLL neuron ground state

To investigate the cellular events that drive the diversification of pLL progenitors into pioneers and followers, we first performed live imaging of pLL neurogenesis. We used the *cldnB:memgfp* transgene to label pLL placodal cells and Tg(*neurod1:Zebrafish*)^{71,72} to visualize pLL progenitors undergoing neurogenesis. Consistent with a previous report³¹, neural (*neurod1*⁺) and sensory progenitors (*neurod1*[−]) were initially intermixed with the pLL placode at the onset of neurogenesis at 15 hpf (Fig. 4A; Supplementary Movie 4). However, within a few hours, *neurod1*⁺ cells delaminated from the pLL placode and migrated anterodorsally, while sensory progenitors moved caudally to form the pLL primordium (Fig. 4B, C). Concurrently, we observed extension of the first few pioneer neurites within the forming pLLP (Fig. 4C, D). Consistent with previous reports^{73,74}, we did not observe cell divisions

among *neurod1*⁺ cells, corroborating the conclusion that neural pLL progenitors are post-mitotic at this stage.

Live imaging revealed several distinct steps in pioneer and follower neuron differentiation, including the onset of neurogenesis (14–15 hpf), separation from sensory progenitors (18 hpf), and initiation of pioneer axon extension concurrent with pLL primordium migration (22 hpf). Thus, we investigated pioneer and follower gene expression dynamics during these critical stages using scRNA-seq. We also included a 48 hpf timepoint to assay whether gene expression differences between pioneers and followers persist at the end of axon extension. *neurod1:egfp*⁺ cells from 14, 18, and 22, and 48 hpf embryos were FAC sorted, sequenced, and combined with those from 30 hpf to identify pLL progenitors (Fig. 5A). Cranial ganglia, CNS and PNS, as well as pancreas were annotated using markers in Fig. S1. Closely clustered cells often reflect differentiation states within a particular lineage⁷⁵. Therefore, we subclustered cells closely associated with pLL neurons (Fig. 5B). The presence of *neurog1*^{11,30,76,77} (an early neurogenesis marker) and absence of *snap25a*^{78,79} (a differentiated neuron marker) indicate that this population represents undifferentiated neural progenitors^{76,80} (Fig. 5C, D). Trajectory inference applied to the scRNA-seq profile of pLL neurons supported this finding⁸¹ (Fig. 5E). Consistently, 14 and 18 hpf cells clustered within the progenitor population, whereas differentiated clusters of pioneers and followers were dominated by cells from 30 and 48 hpf (Fig. 5F).

To analyze expression dynamics during pLL neurogenesis, we examined pioneer (*rpz5* and *ret*) and follower (*hoxb5a* and *zfhx3*) markers (Fig. 5G–J). Follower markers were expressed in most pLL progenitors at 14, 18, and 22 hpf (Fig. 5I, J). In contrast, pioneer markers were largely absent at 14 hpf and were expressed by only a small subset of cells at 18 and 22 hpf (Fig. 5G, H). Interestingly, we observed several *neurog1*-positive progenitors at 30 hpf (Fig. 5F). These presumably represent previously described, later-born neurons that innervate secondary trunk NMs after 2 dpf⁷³. As these late progenitors do not contribute to pioneer neurons, we focused our analysis on 14, 18, and 22 hpf stages.

Co-expression analysis revealed a number of cells containing both follower and pioneer markers at these three stages (Fig. 5K, L), potentially indicating a transitional state. To more broadly analyze the expression of pioneer and follower genes at these early stages, we generated pioneer and follower marker gene signatures (top 20 upregulated genes at 30 hpf in each population) using the AddModuleScore function in Seurat. The follower gene signature was present broadly in cells from early timepoints (Fig. 5M), whereas the pioneer gene signature was present only in a few 22 h cells at the end of the differentiation trajectory (Fig. 5N). Consistent with these observations, follower gene expression was maintained at similar levels over time—initially in progenitors and subsequently in followers—whereas pioneer genes were upregulated during the later stages of neurogenesis (Fig. 5O).

Finally, we observed that transcriptional differences between pioneers and followers persisted at 48 hpf, after initial axon extension had concluded (Fig. 5F). Altogether, these experiments showed that

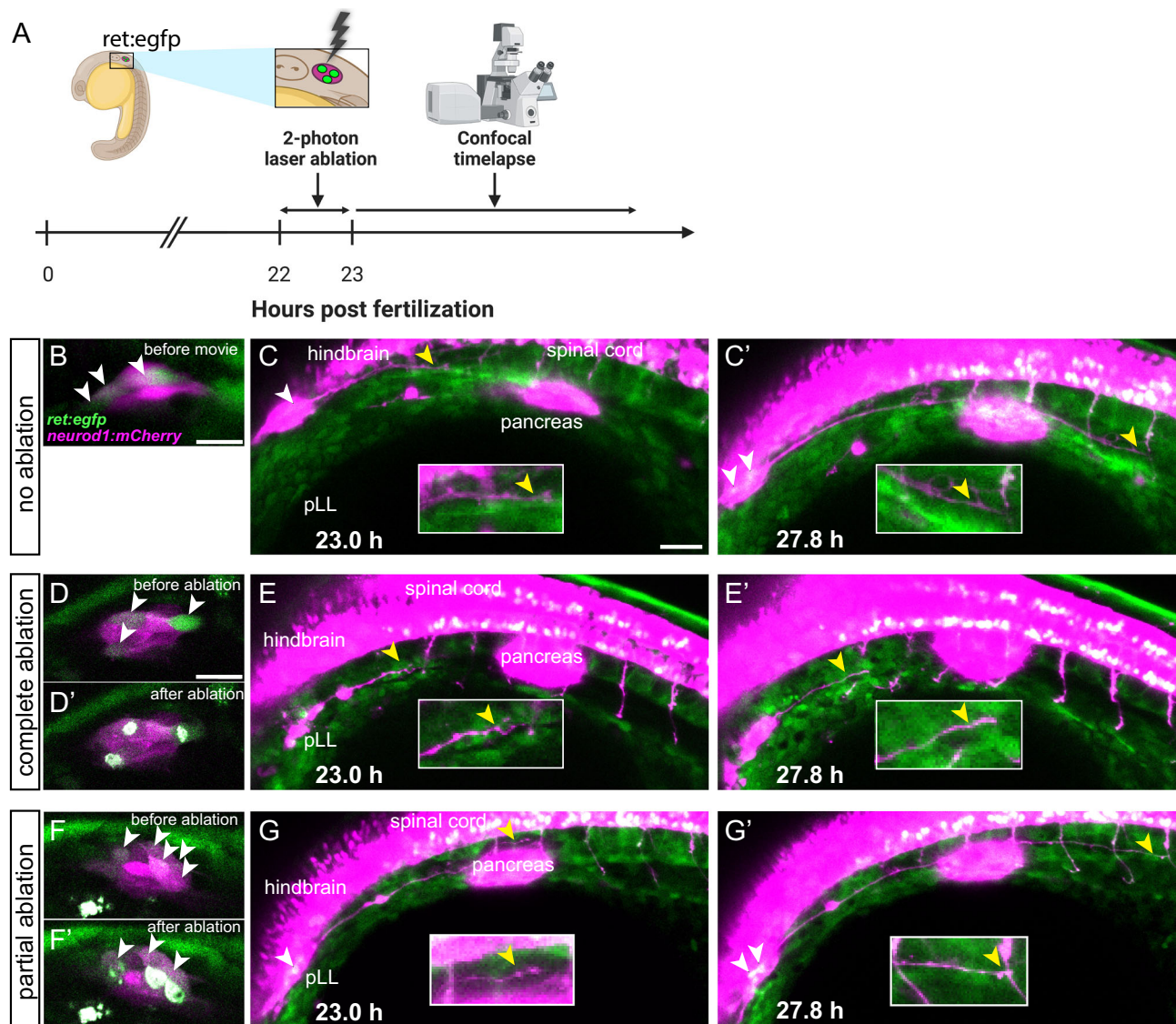


Fig. 3 | pLL pioneer neurons are required for follower axon extension.

A Schematic depicting ablation strategy. EGFP+ neurons were ablated between 22 and 23 hpf and then imaged live using confocal microscopy. Created in BioRender. Lab, N. (2025) <https://BioRender.com/vij5z6b>. **B** Non-ablated pLLg at 22 hpf immediately before timelapse begins. **C** Stills from timelapse of the control embryo shown in (B) at 23 hpf (C) and 27.8 hpf (C'). **D** pLLg before and after (D') ablation of

all three EGFP+ neurons. **E** Stills from timelapse recorded after complete ablation in (D). **F** pLLg before and after ablation (F') of three out of five EGFP+ neurons. **G** Stills from timelapse recorded after partial ablation in (F). White arrowhead = EGFP+ pLL neurons; yellow arrowhead = pLL nerve terminals. All scale bars = 20 μm. All images scaled the same.

follower-specific markers are expressed in early differentiating pLL progenitors, defining the pLL ground state. They further suggest that pioneers represent a later developmental state derived from follower progenitors. Additionally, we concluded that pioneers and followers maintain distinct transcriptional profiles through the completion of pioneer axon extension.

Pioneer precursors exhibit distinct cellular behavior

To identify pioneer precursors and to confirm the presence of a follower-to-pioneer transitional state in vivo, we used FISH to visualize expression of pioneer (*ntnk1*) and follower (*nr2f2*) genes at early timepoints between 14 and 20 hpf (Fig. 6A–C). The *cldnB:memgfp* transgene marks all pLL placode cell membranes, while the *neurod1:mCherry* transgene marks pLL progenitors undergoing neurogenesis. Consistent with scRNA-seq, mCherry-positive neuroblasts expressed *nr2f2* but not *ntnk1* at the onset of neurogenesis (Fig. 6A). Within the next 2 hours (15–17 hpf), we observed a few *ntnk1*+/*nr2f2*- cells in the process of delamination from the placode (cells marked by

arrows in Fig. 6B, C). Simultaneously, several cells within the placode coexpressed both *ntnk1* and *nr2f2* (cells marked by arrowheads in Fig. 6B, C). Overall, 17.0% of cells coexpressed *ntnk1* and *nr2f2* between 14 and 20 hpf (Fig. 6D), whereas at 30 hpf coexpression was rare, at only 1.8% (Fig. 6E). These observations suggest that pioneer neuron precursors delaminate first from the pLL placode after transitioning from a follower ground state.

To observe this process in real time, we marked leading delaminating cells by photoconversion in the *Tg(neurod1:Kaede)^{nl29}* (hereafter, *neurod1:kaede*) transgenic line and followed these cells by live imaging to visualize their axon terminals (Fig. 6F–H; Supplementary Movie 5). After delaminating, these cells displayed a multipolar morphology that changed to spindle-like, just prior to extending their neurites. Marked cells consistently became pioneer neurons (*n* = 4 of 4 cells; Fig. 6H). We next labeled cells within the more distal region of the pLL placode. As evidenced by their axons lagging behind the pLLP (Fig. 6I–K; Supplementary Movie 6), most of these cells became followers (*n* = 7 of 9 cells; Fig. 6L).

We also used an alternative method to visualize both differentiating pioneer and follower precursors. One-cell stage *cldnB:memgfp* embryos were injected with a *neurod:mCherry* construct. Because the incorporation of plasmid during development is stochastic, we screened for embryos with mosaic *mCherry* expression in a small number of pLL cells to visualize cellular morphology and behavior. Differentiating pLL neurons exhibited two distinct behaviors. One subset rapidly adopted a spindle-like morphology by 17–18 hpf and extended a peripheral neurite that invaded the field of differentiating sensory progenitors (Fig. 6M–O; Supplementary Movie 7). These neurites remained within the field of sensory pLL progenitors, and long-term tracking of these neurons identified them as pioneers (Fig. 6O; Supplementary Movie 7). Interestingly, pioneer precursors were positioned anterodorsally, consistent with our previous observation that these cells are the first to delaminate.

In contrast to pioneers, follower precursors maintained a dynamic multipolar morphology until late stages of neurogenesis (Fig. 6P–R; Supplementary Movie 8). At ~20 hpf, they began extending their

peripheral neurites; however, they never invaded the field of sensory progenitors (Fig. 6P; Supplementary Movie 8). These cells were positioned posteroventral to pioneers and close to sensory progenitors, presumably due to delaminating later than pioneers. Overall, these data suggest that pioneer precursors first enter a transitional state, followed by upregulation of *ntnr1* and delamination. During this process, they initially display multipolar behavior, but then rapidly adopt a bipolar morphology and extend their peripheral neurites well before follower precursors do.

Downregulation of retinoic acid is required for proper pioneer axon targeting

We next sought to examine molecular signals that regulate pioneer and follower neuron differentiation. Because pioneer precursors appear to enter a transitional state in which follower genes are downregulated, we searched for a pathway that was active in early pLL progenitors but absent in pioneers. We noted that RA pathway member *crabp1b*⁴⁴ and known transcriptional targets of RA in other systems, *hoxb5a*, *nr2f2*, and *zfhx3*^{45,58–60}, were expressed in pLL progenitors between 14 and 22 hpf (Fig. 5I, J, O, and Fig. S7). Interestingly, scRNA-seq also revealed that the pathway remained active in followers, but not in pioneers, during axon extension stages (Fig. 5I, J). Thus, we asked whether *hoxb5a*, *nr2f2*, and *zfhx3* act downstream of RA signaling in the pLL neurons. To address this, we mosaically overexpressed either constitutively-active RAR (caRAR-2A-EGFP-CAAX, hereafter caRAR) or dominant-negative RAR (dnRAR-2A-EGFP-CAAX, hereafter dnRAR) constructs and evaluated animals with individually labeled pLL neurons for expression of the three genes at 30 hpf (Fig. S8A–F). Modulation of RA signaling had no significant effect on *nr2f2* or *zfhx3* expression levels. In contrast, activation of RA increased, and inhibition of RA decreased, *hoxb5a* expression levels (Fig. S8G–J). These results indicate that *hoxb5a*—but not *nr2f2* or *zfhx3*—is an RA target in pLL neurons.

Next, we asked whether RA signaling plays a role in pioneer neuron differentiation. Using the same strategy, we mosaically overexpressed caRAR, dnRAR, or EGFP-CAAX (control) and evaluated animals with individually labeled neurons for pLL axon targeting at 72 hpf as a proxy for pioneer differentiation (Fig. 7A, B–G). Control neurons expressing EGFP-CAAX projected randomly between L1 and terminal cluster NMs (Fig. 7H). Activation of the RA pathway via caRAR expression caused a striking shift in axonal targeting toward proximal neuromasts (Fig. 7F, H), which are known targets of follower neurons^{11,24,27}. Notably, none of these labeled neurons projected to the

Table 1 | Ret+ pioneer neurons are required for the pLL nerve extension

Embryo	Condition	Axial change (somites migrated, 23–28 hpf)
1	Nonablated	7
2	Nonablated	6
3	Nonablated	7
4	Nonablated	6
5	Nonablated	6
6	Nonablated	8
7	Nonablated	7
8	Complete	1
9	Complete	1
10	Complete	0
11	Complete	2
12	Complete	0
13	Partial (3 of 5)	5
14	Partial (6 of 7)	2

Means between nonablated controls and complete ablations are statistically significant: $p = 0.0013$ (one-tailed Mann-Whitney non-parametric test).

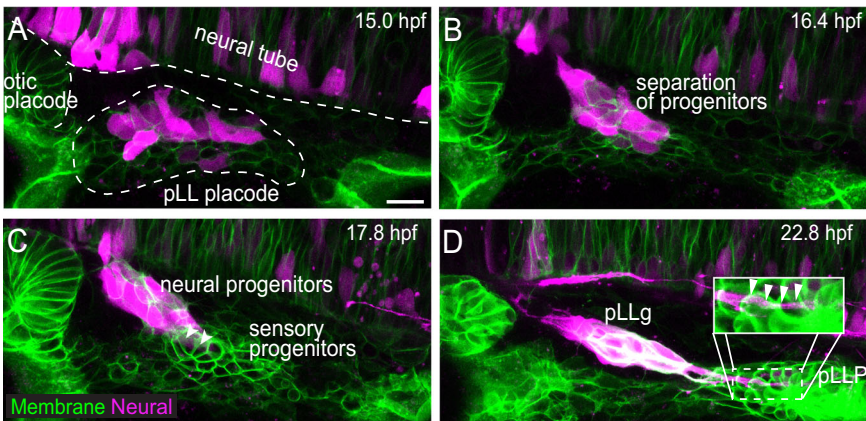
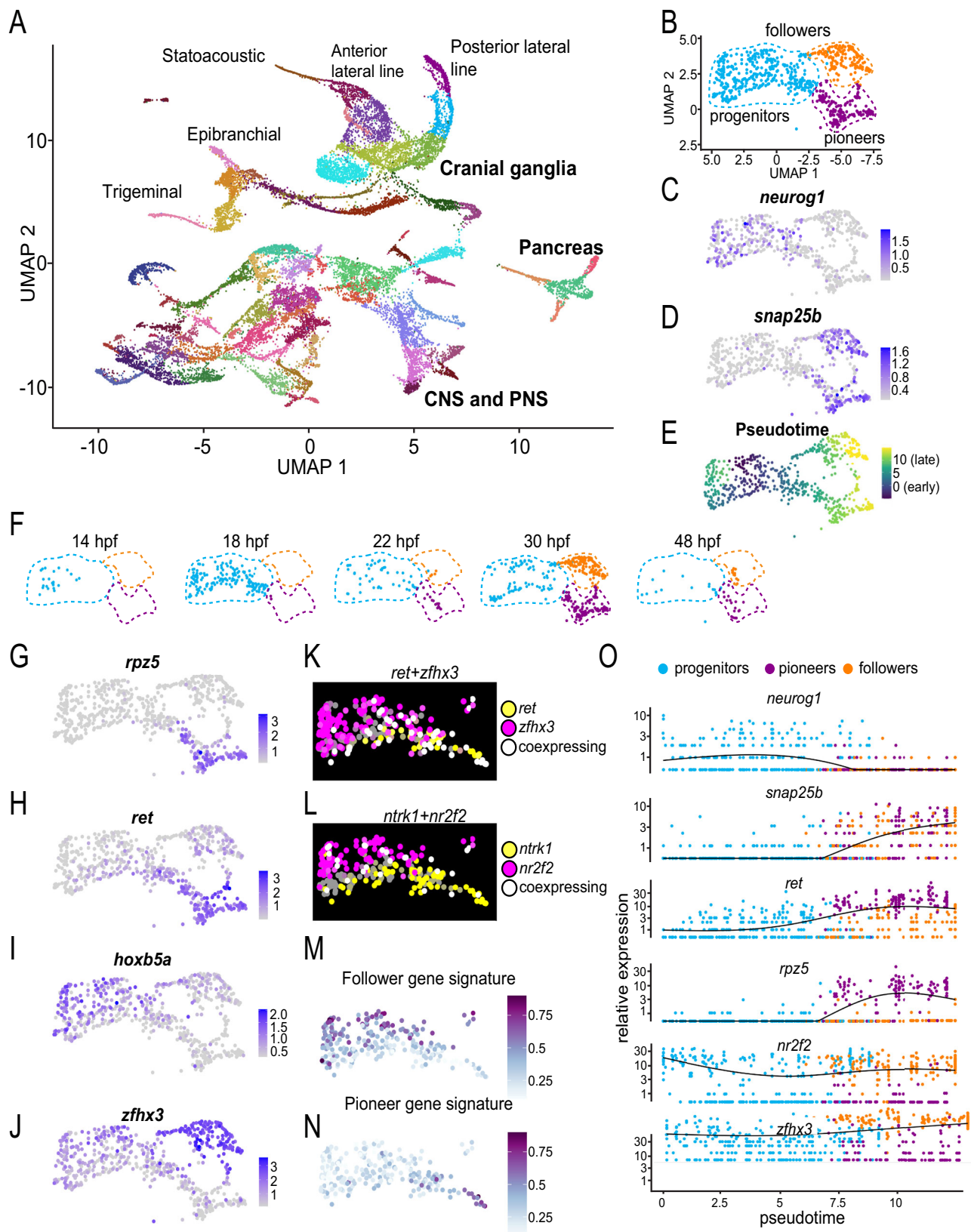


Fig. 4 | Live imaging defines cellular events during pLL morphogenesis. **A–D** Stills from a timeseries (Supplementary Movie 4) visualizing formation of the pLL system between 15 and 23 hpf. The pLL placode is marked by the *cldnB:memgfp* transgene, while pLL progenitors undergoing neurogenesis are visualized by *Tg(neurod1:Zebrafish)*. The pLL placode, otic placode, and the neural tube are outlined by dashed lines. **A** At the onset of pLL neurogenesis (15 hpf), neural and

sensory progenitors are intermixed within the pLL placode. **B** Neural and sensory progenitors are in a process of separating from the pLL ganglion and primordium, respectively. **C** Neural and sensory progenitors separate at 18 hpf, while neurites (arrowheads) from pLL progenitors project toward sensory progenitors. **D** At 22 hpf, pioneer axons (marked by arrowheads in the inset) extend with the migrating pLLP. Scale bar = 10 μm . All images scaled the same.



terminal cluster, which is typically targeted by pioneers. In contrast, repression of RA signaling using dnRAR caused axons to preferentially innervate distal NMs (Fig. 7H). This bias in axon targeting indicates that active RA signaling within pLL neurons promotes innervation of follower targets, while attenuation of RA signaling biases neurons toward innervation of pioneer targets.

Retinoic acid negatively regulates *ret* and is critical for correct pioneer neuron axon targeting

We next aimed to identify a mechanism by which RA directs pLL axon targeting. Our previous study demonstrated that the neurotrophin factor receptor *ret* regulates pLL axon extension. *ret* mutant embryos exhibit a nerve truncation phenotype: proximal NMs are innervated

Fig. 5 | Follower is a transcriptional ground state of pLL progenitors. **A** UMAP plot of all cells derived from 14, 18, 22, 30, and 48 hpf *neurod1:egfp* embryos. Major cell types are indicated. **B** UMAP of the pLL progenitors, pioneers, and followers. **C, D** Feature plots showing neurogenesis marker, *neurog1*, and neural differentiation marker, *snap25b*. **E** Trajectory inference plot showing the predicted differentiation trajectory, consistent with the expression patterns of neurogenesis and differentiation markers in (**C, D**). **F** UMAP plot of pLL progenitors, pioneers, and followers grouped by timepoint. The pLL cell counts at each timepoint are as follows: 14 hpf, 23 cells; 18 hpf, 167 cells; 22 hpf, 67 cells; 30 hpf, 340 cells; and 48 hpf, 50 cells. **G, H** Pioneer markers *rpz5* and *ret* are predominantly expressed in pioneers, but not in progenitors. **I, J** Follower markers *hoxb5a* and *zfhx3* are

expressed in both progenitor and follower populations. **K, L** Feature plots showing coexpression of pioneer (*ret* or *ntkr1*) and follower (*zfhx3* or *nr2f2*) genes during differentiation (14–22 hpf). Note that a subset of cells coexpress both pioneer and follower markers at these stages (white cells): 25 cells co-express *ret* and *zfhx3*, and 25 cells co-express *ntkr1* and *nr2f2*. Low expression cut off is set at 3 UMI per cell. **M, N** Gene signature plots of cells between 14 and 22 hpf. The follower gene signature is present broadly at earlier stages, while the pioneer gene signature is strongest in cells from 22 hpf. **O** Gene expression over time as cells differentiate from progenitors to followers or pioneers. Note that follower gene expression is similar across stages, whereas pioneer genes are upregulated during later differentiation stages.

normally but most terminal NMs are not⁵. Accordingly, we investigated whether RA regulates *ret* expression in pLL neurons. Using the same strategy, we mosaically overexpressed EGFP (control), caRAR, or dnRAR. We then fixed these embryos at 30 hpf and performed FISH to measure *ret* and *hoxb5a* (positive control) expression levels in EGFP-positive neurons (Fig. 8A–E). As expected, *hoxb5a* became almost undetectable in neurons expressing dnRAR. Conversely, RA activation via caRAR significantly increased expression of *hoxb5a* (Fig. 8A–D). In EGFP expressing controls, we observed two groups of *ret*-expressing cells: *ret* high and *ret* low, presumably corresponding to pioneers and followers, respectively (Fig. 8E). However, neurons expressing caRAR showed comparably lower levels of *ret* (Fig. 8B, E), while neurons expressing dnRAR exhibited elevated levels of *ret* (Fig. 8C, E).

We next asked whether RA regulates *ret* expression through *Hoxb5a*. To disrupt *hoxb5a*, we injected a combination of three CRISPR guides targeting the *hoxb5a* locus (Fig. S9A). Oxford Nanopore sequencing of the locus in the injected embryos (crisprants) revealed that the biallelic knockdown frequency was 99.32% (individual guide frequencies were 73, 93, and 82%; Fig. S9A). We found that *ret* expression was significantly increased in *hoxb5a* crisprants at 30 hpf (Fig. S9B–D). Altogether, these results demonstrate that RA signaling, through *Hoxb5a*, negatively regulates *ret* levels in pLL neurons.

Previous studies have shown that RA and Fgf signaling pathways can antagonize each other during development, including during pLL placode induction^{32,82–85}. To determine whether this interaction occurs in the pLL during neuronal specification, we treated embryos with 75 μ M SU5402, a well-characterized Fgf receptor inhibitor⁸⁶, between 14–18 or 14–20 hpf and assayed for *ret* and *hoxb5a* expression (Fig. S10A–D). While *hoxb5a* was unchanged, *ret* expression was increased at 18 hpf, but not at 20 hpf (Fig. S10E–H). Thus, while Fgf signaling regulates *ret* expression during initial stages of the pLL development, it appears to do so independently of RA.

Based on the axon targeting bias resulting from RA modulation (Fig. 7H) and the associated changes in *ret* expression, we asked whether *ret* acts downstream of RA to direct pioneer axon targeting. To test this, we again used mosaic overexpression and compared axon targeting of pLL neurons expressing caRAR and *mCherry* to those expressing caRAR and *ret-mCherry*⁵ (Fig. 8F). As expected, we observed a dramatic increase in neurons projecting toward proximal targets among caRAR;*mCherry* positive neurons (Fig. 8G, H, and K) while none projected beyond NM L4. Overexpression of *ret-mCherry* with caRAR repressed this effect: these neurons exhibited a strong bias toward distal targets (Fig. 8I, J, and L). These experiments demonstrate a mechanism by which RA regulates innervation of peripheral pLL axons: elevated levels of RA direct axons towards proximal sensory organs, whereas low RA signaling directs pioneer axons to distal sensory organs via the neurotrophin factor receptor *ret*.

Discussion

Summary and novelty of study

The term “pioneer neurones” was first coined in 1976¹. Since then, they have been the subject of extensive research investigating their unique characteristics. While their morphological and behavioral properties

have been well described in many model systems, a comprehensive molecular analysis has remained elusive due to the lack of genetic tools to specifically label pioneers. As a result, although some differentially expressed genes have occasionally been reported, it has remained unclear whether pioneers constitute a molecularly distinct cell type from followers. Here, using single-cell transcriptomics, we present the first global transcriptional profile of pioneer and follower neurons, revealing that pioneers possess a unique molecular signature that underlies at least some of their distinct migratory and navigational behaviors. We further demonstrate that pioneers arise from a neural progenitor pool with a default follower identity, indicating that the pioneer subtype is acquired later. In addition, we show that pLL pioneers are essential for follower axon extension. Finally, our results reveal that modulation of RA signaling biases axonal innervation of pLL neurons toward either pioneer or follower targets. Collectively, this evidence establishes that pioneers and followers are not merely functional states but represent transcriptionally and functionally distinct neuronal subtypes.

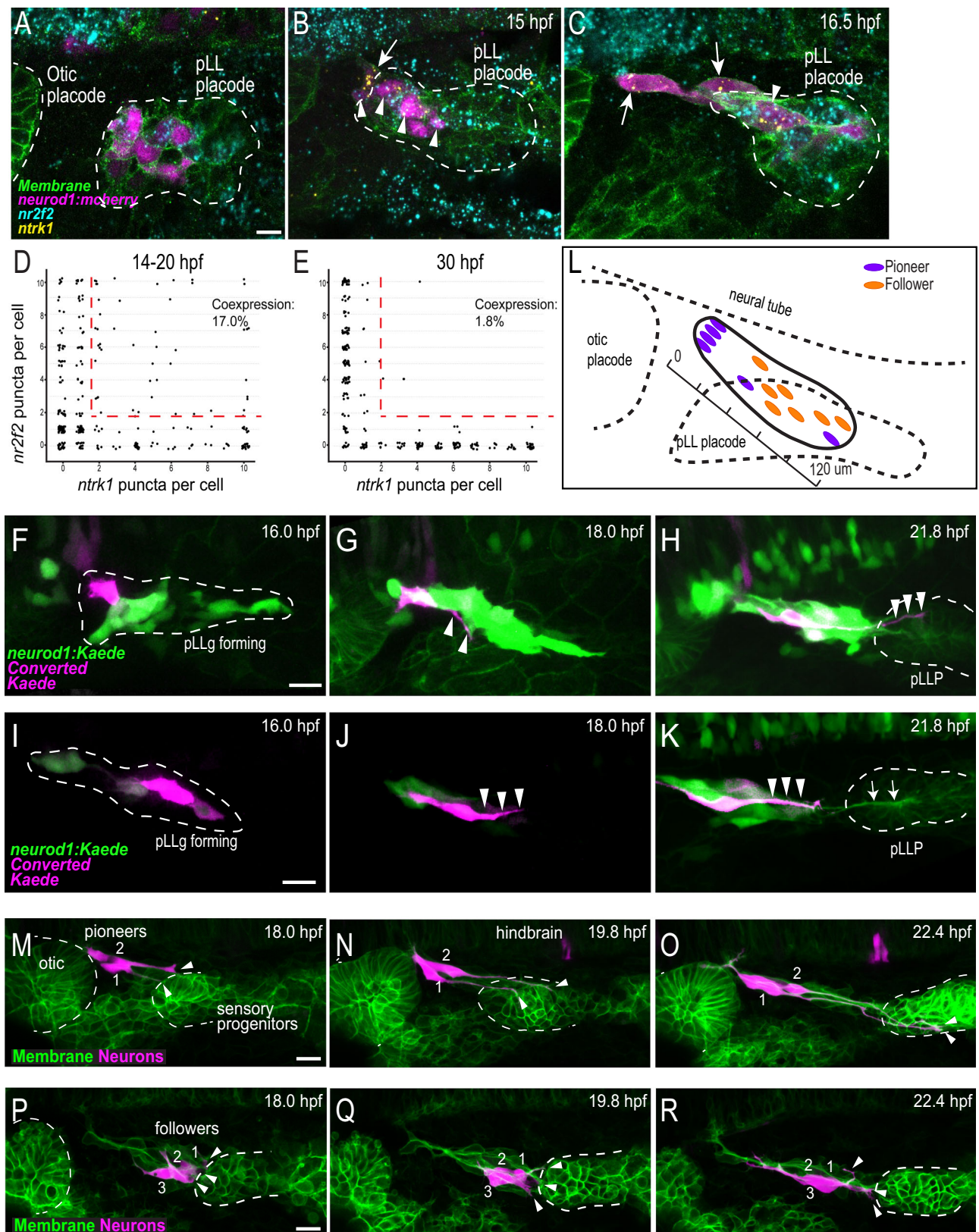
A model of pioneer versus follower lineage specification

We found that the transcriptional profile of pLL progenitors is strikingly similar to followers: progenitors express a number of genes that then persist in follower neurons during later stages. The pioneer transcriptional state, on the other hand, appears to be acquired after pLL neuroblasts exit the pLL placode. Live imaging experiments showed that the cells fated to become pioneers tend to delaminate from the pLL placode first; they initially exhibit a multipolar morphology, which transitions to a spindle-like shape. These cells also move anterodorsally and were the first to exhibit detectable expression of pioneer marker *ntkr1*. The reproducible, spatiotemporal specification of pioneers suggests that instructive signaling occurs early during neurogenesis. However, it remains unknown whether pioneer fate is induced by an external signal or by the escape of an inhibitory signal produced within the placode during delamination.

One potential candidate is Fgf. For example, the neural tube secretes Fgf ligands that are required for the induction of the otic and epibranchial placodes at this stage^{55,87,88}. Given the proximity and direction of pioneer precursor migration, it is possible these cells are exposed to Fgf ligands. In support of this idea, we found that Fgf signaling is required for expression of *ret*, an early pioneer marker (Fig. S10). Additionally, Fgf and RA form countervailing gradients to regulate neural^{82,83} and pLL induction³². However, this mechanism is unlikely to be engaged during pLL neurogenesis, as inhibition of the Fgf signaling did not affect *hoxb5a*, a transcriptional target of RA. Future studies will uncover signaling mechanisms that induce pioneers from the progenitor ground state.

Regulation of the pLL pioneer development by RA

During development, RA is required for the formation of the pLL placode³². Thus, it is not surprising that RA is active in all pLL progenitors. We also found that downregulation of RA signaling, as well as its transcriptional target, *hoxb5a*, in maturing pLL neuroblasts is necessary for the expression of at least one pioneer gene, *ret*. This, in



turn, is required for proper innervation of pioneer targets. This raises the question of the specific mechanism leading to downregulation of RA in pioneers. RA is produced in paraxial mesoderm during somitogenesis and acts as a morphogen controlling A-P embryonic patterning, primarily through the transcriptional regulation of Hox genes^{32,36,57,58,89}. However, the population of neural pLL progenitors is

relatively small (~20 cells) at the time of differentiation; thus, it seems unlikely that a substantive morphogenic gradient could be established within such a confined space. In addition, neural progenitors within the pLL placode are not uniformly distributed (Fig. 4A)³¹, further complicating the notion of morphogen-based instruction in this system. Instead, pioneer precursors may actively downregulate intracellular

Fig. 6 | Pioneer precursors exhibit distinct cellular behavior. **A–C** A single confocal Z-slice through the pLL ganglion labeled with FISH probes against *ntnr1* (yellow) and *nr2f2* (cyan) between 14 and 16.5 hpf. Cell membranes are labeled by *cldnb:mengfp*, whereas pLL neuroblasts are marked by *neurod1:mCherry*. Dashed line outlines pLL and otic placodes. Arrows mark leading tip cells upregulating pioneer marker *ntnr1*. Arrowheads mark neuroblasts co-expressing *ntnr1* and *nr2f2* (two replicates; $n = 10$ total animals). **D, E** Quantification of *ntnr1* and *nr2f2* expression between 14 and 20 hpf (**D**) or 30 hpf (**E**). Dashed red lines indicate cells that coexpress both markers. Note the significant number of co-expressing cells at 14–20 hpf (51/300 cells; 17%) compared to 30 hpf (5/285 cells; 1.8%); $p = <0.001$, Chi-Square test. **F–H** Stills from a time series using *neurod1:kaede* photoconversion at 16 hpf. **F–H** The first delaminating tip cell was photoconverted and tracked to visualize its peripheral axon. Note that the axon projects into the pLLP. Arrowheads = photoconverted axons, arrows = pioneer axons. **I–K** A photoconversion of a distal cell. Note the labeled axons lagging behind the pLLP. Arrowheads =

photoconverted axons, arrows = pioneer axons. **L** Schematic summary of photoconversions at 16 hpf. Cell location shows the region where it was photoconverted, and color indicates whether it became pioneer or follower. Delaminating tip cells became a pioneer 4 of 4 times. In labeled distal cells, 7 of 9 became followers, and 2 became pioneers. **M–O** Stills from a timeseries of two individually labeled neurons between 17 and 25 hpf. **M** Anterodorsal neurons appear spindle-shaped with early neurite projections. **N** Their pioneer neurites localize within the pLLP. **O** Pioneer neurons extend their axons with the primordium during migration. Pioneer neurites marked by arrowheads. **P–R** Stills from a timeseries of three individually labeled neurons beginning at 17 hpf. Note the absence of neurites in the pLLP through the time series. Follower neurites marked by arrowheads. For experiments shown in (**M–R**), we imaged 7 embryos that contained 4 pioneers and 7 followers. Membrane = *cldnb:mengfp* (green). All scale bars = 20 μm . All images scaled the same.

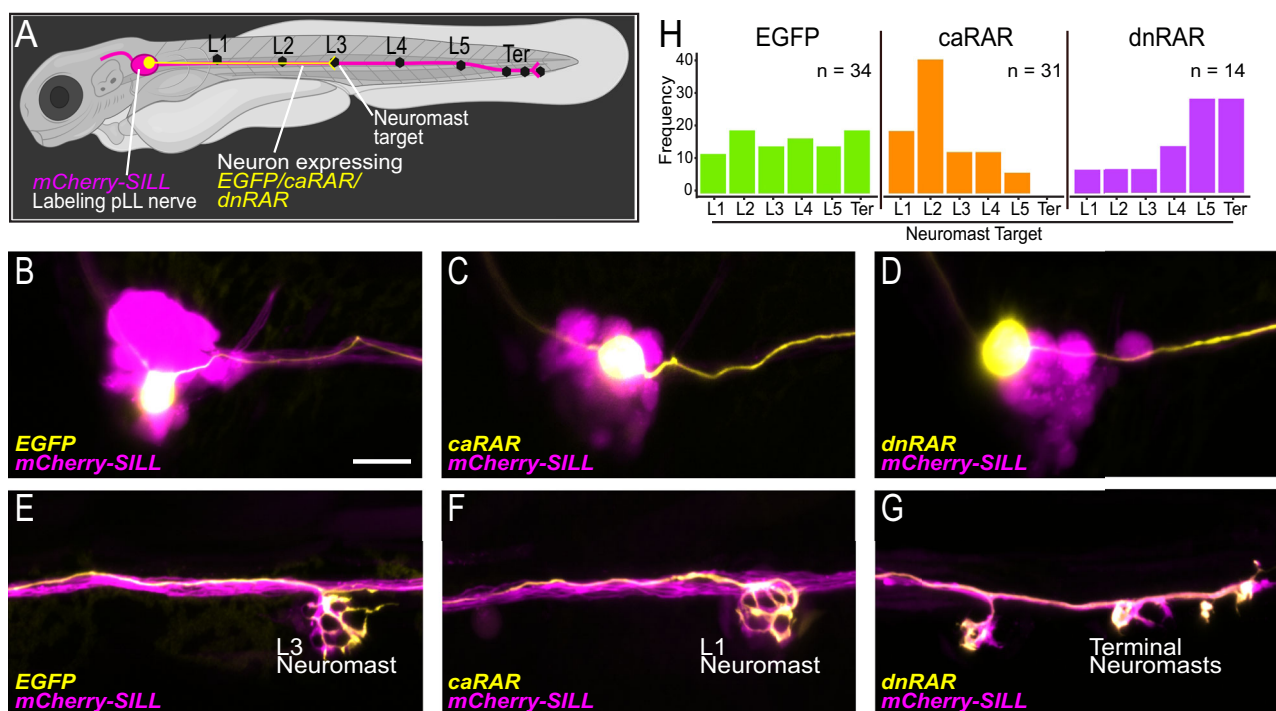


Fig. 7 | Retinoic acid regulates pioneer neuron axon targeting. **A** Schematic of mosaic labeling strategy. *Tg(hsp70l:mCherry, en.sill)*ⁿ³⁰ embryos were injected with one of the following plasmids: *SILL:EGFP-CAAX*, *SILL:caRAR-CAAX*, or *SILL:dnRAR-CAAX* at the one-cell stage. Animals were grown to 3 days and assessed for the presence of single EGFP-positive neurons in the pLL ganglion and the location of EGFP-positive axon terminals. Created in BioRender. Lab, N. (2025) <https://BioRender.com/vij5z6b>. **B–G** Representative confocal images of single labeled neurons in the pLLg and their targets following overexpression of *EGFP* (**B, E**),

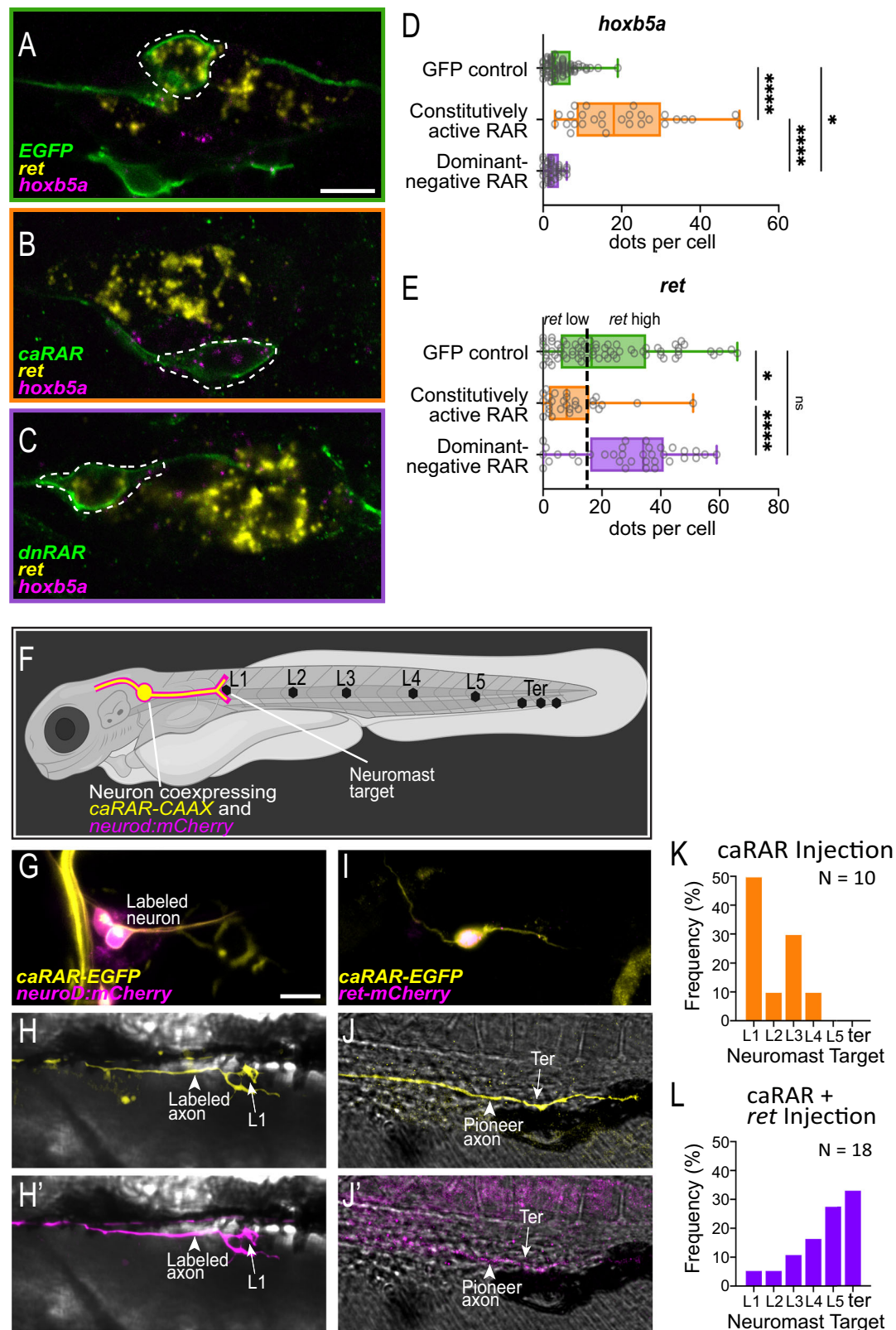
caRAR (**C, F**), or *dnRAR* (**D, G**). The following number of cells were examined in 3 independent experiments (1 cell/animal): EGFP – 34; caRAR – 31, and dnRAR – 14. **H** Frequency of neuromast targeting along zebrafish trunk by neurons labeled with *EGFP*, *caRAR*, or *dnRAR*. Difference in axon targeting assessed by Chi-Square: EGFP vs. *caRAR* $p = 0.0011$; EGFP vs. *dnRAR* $p = 0.0795$; *caRAR* vs. *dnRAR* $p = 0.0001$. All images are lateral views with anterior to left. Scale bars = 20 μm . All images scaled the same.

RA signaling as they exit the pLL placode. The mechanisms by which RA is differentially regulated in pLL pioneer and follower neurons will be addressed in future studies.

Our analysis revealed that Ret functions downstream of RA in pLL axon targeting, as overexpression of Ret is sufficient to suppress the effects of RA activation in pLL neurons. However, it remains unclear to what extent RA might more broadly governs pioneer cell fate. RA typically regulates many transcriptional targets, so it is plausible that pioneer genes are expressed as a result of RA pathway downregulation. One interesting alternative is the potential regulation of pioneer genes by Ret via retrograde signaling. It is known that in pLL axons, activated Ret is retrogradely transported to the cell body, where it can regulate gene transcription⁵. It is possible, then, that Ret initiates a broader signaling cascade to activate a pioneer-

specific genetic program. More studies are necessary to uncover whether pioneer cell fate is regulated by modulation of RA. Alternatively, inhibition of RA may specifically regulate pioneer axon targeting without affecting specification.

It appears that the function of RA signaling—to inhibit axon extension—is conserved in at least one other developmental context⁴³. The first neurons to innervate pharyngeal arches, vagal pioneer motor neurons, are regulated by a receding wave of RA such that the timing of expression of key axon outgrowth genes is initiated by RA decline⁴³. In this system, RA reduction resulted in vagal neuron expression of the neurotrophin receptor *met*, enabling axons to respond to target-derived hepatocyte growth factor (HGF) in the pharyngeal arches. Thus, in both systems, neural precursors require the downregulation of RA to initiate axon outgrowth.



Do pioneer and follower neurons retain molecular differences over time, after the initial axon extension is complete?

Are pLL pioneers and followers merely transient neuronal identities, or do their differences persist beyond developmental stages? Our analyses focused on the period between early neurogenesis (14 hpf) and the end of axon extension (48 hpf), prior to activation of the pLL circuit (72 hpf). Notably, previous studies have identified two

physiologically distinct circuits in the pLL: one innervating distal tail NMs (large-caliber, fast-conducting pioneers), and the other innervating more proximal NMs (innervated by small-caliber, slower-conducting followers)^{10,11}. This is not surprising, as there are mechanical differences in hydrodynamics between the tail, where water flow is quicker, and the trunk, where flow is steadier⁹⁰. Accordingly, patch clamp recordings showed that a higher level of stimulation was

Fig. 8 | Retinoic acid negatively regulates *ret*. **A–C** Representative single confocal Z-slices of pLL ganglia expressing *EGFP* (**A**), *caRAR* (**B**), or *dnRAR* (**C**) in individual cells (dashed outlines). Expression of *ret* (yellow) and *hoxb5a* (magenta) was assessed by FISH. **D, E** Quantified expression levels of *hoxb5a* and *ret* after injection of RAR constructs. We analyzed the following numbers of embryos from two independent experiments: EGFP control: 21; *caRAR*: 15; *dnRAR*: 12. Each plot shows minimum, Q1, median, Q3, and maximum. Nonparametric Kruskal–Wallis test values are shown on plots: * $p < 0.05$; **** $p < 0.0001$. Exact p -values are as follows: *hoxb5a*, GFP vs *caRAR* < 0.0001 ; GFP vs *dnRAR* = 0.0340; *caRAR* vs *dnRAR* < 0.0001 ; *ret*, GFP vs *caRAR* = 0.0135; GFP vs *dnRAR* = 0.1024; *caRAR* vs *dnRAR* < 0.0001 . **F** Schematic of mosaic labeling using coinjection of two constructs: *caRAR*-2A-EGFP and *mCherry* (control) or *caRAR*-2A-EGFP and *ret-mCherry* driven by

neurod1 promoter. Following injection, embryos were screened at 72 hpf for the position of colabeled axon terminals. Created in BioRender. Lab, N. (2025) <https://BioRender.com/vij5z6b>. **G, H** Confocal image of the neuron cell body (**G**) and its axon terminal (**H**) labeled by *caRAR* and *mCherry* (H,H'). **I, J** Confocal image of the neuron cell body (**I**) and its axon terminal (terminal NMs) labeled by *caRAR* and *ret-mCherry* (J,J'). **K, L** Frequency of NM targeted by labeled neurons coexpressing either *caRAR*-2A-EGFP+*mCherry* or *caRAR*-2A-EGFP + *ret-mCherry*: $p = 0.0002$, Chi-square test. The following number of cells were examined in 2 independent experiments (1 cell/animal): *caRAR*-2A-EGFP + *mCherry* – 10; *caRAR* – 10, and *caRAR*-2A-EGFP + *ret-mCherry* – 18. All images are lateral views with anterior to the left. Scale bars = 20 μ m. All images scaled the same.

required in the distal neuromast (L5) compared to the proximal neuromast (L2)¹⁰. In conclusion, the molecular differences we identified, combined with the distinct physiological properties of circuits formed by pioneers and followers, support the idea that pLL pioneers and followers maintain distinct identities even after mature circuits are established.

Is pioneer cell state molecularly distinct in other systems?

We were able to transcriptionally distinguish pioneers and followers in the pLL as distinct subpopulations. Is there evidence from other systems that pioneers and followers represent discrete cell types? One argument supporting this idea comes from the result of ablation or replacement experiments demonstrating that followers cannot compensate for pioneer function in other systems. We showed that in the pLL, pioneer ablation leads to a complete halt of nerve extension, indicating that followers cannot compensate for pioneers in this system. Similar results have been reported in the *Drosophila* ventral nerve cord⁶⁷, zebrafish spinal neurons^{91,92}, and mammalian CNS^{93,94}. Thus, multiple studies lend credence to the notion that pioneer neurons have a unique molecular profile that endows them with capabilities absent in follower neurons.

In summary, our work reveals that pLL pioneer neurons exhibit significant molecular differences compared to followers. Importantly, key features of pioneer behavior and morphology are conserved across multiple systems. However, whether this translates into transcriptional similarity among pioneers across different systems is yet to be determined. Our work provides a foundation for identifying the mechanisms by which pioneer neurons arise and are specified, which will enhance our broader understanding of pioneer neurons. Finally, identifying the main factors regulating pioneer neuron fate commitment and differentiation will generate a list of novel therapeutic targets for research on nerve injury and regeneration.

Methods

Oligo sequences and key reagents are summarized in Supplementary Tables 2 and 3.

Animal husbandry

All experiments were approved by the Institutional Animal Care and Use Committee at Oregon Health & Science University (Protocol #TR03_IP00000495). Adult zebrafish were maintained at 28.5 °C. Embryos were derived from natural matings and were raised in embryo medium either at 28.5 °C (standard) or at 23.5 °C (to slow development). Embryo staging was conducted according to Kimmel et al.²². Strains utilized in this study were *AB, TgBAC(*neurod1:egfp*)^{nl1}, Tg(-8.0cldnB:LY-EGFP)^{zfl06}, TgBAC(*ret:EGFP*)^{h1331}, Tg(*rpz5:mRuby*)^{nl27}, Tg(*5kbneurod1:mCherry*)^{nl28}, Tg(*prim:lyn2-mCherry*)²⁹, Tg(*neurod1:kaede*)^{nl29}, and Tg(*hsp70l:mCherry, en.silll*)^{nl30}.

Embryo dissociation

TgBAC(*neurod1:egfp*)+ embryos were dissociated following a modified version of the protocol from the Lawson lab⁹⁵. Briefly, 1.2 mL of

protease solution (0.25% trypsin, 1 mM EDTA, pH 8.0 in PBS) was warmed in a 24-well plate at 28.5 °C for 10 min. Embryos were then transferred to a 1.5 mL tube and embryo media was removed and replaced with 100 μ L of calcium-free Ringer's solution. Embryos were de-yolked by gentle pipetting 15 times with a p200, then transferred to the warmed protease solution. 27 μ L of Collagenase P/HBSS (160 U/mL) was added followed by pipette mixing. Plates were incubated at 28.5 °C for 15 min with trituration every 5 min by pipetting with a p1000. Digestion was halted by addition of 6x stop solution (30% calf serum, 6 mM CaCl₂, PBS), and the entire volume of each well was transferred to a microcentrifuge tube. Tubes were spun at 350 x g at 4 °C for 5 min and supernatant was removed. The cell pellet was rinsed by adding 1 mL chilled suspension solution (1% FBS, 0.8 mM CaCl₂, 50 U/mL penicillin, 0.05 mg/mL streptomycin, DMEM) and then spun down again at 350 x g at 4 °C for 5 min; the supernatant was removed. The cell pellet was resuspended in 700 μ L suspension solution and passed through a 40 μ m cell strainer into a FACs tube on ice.

FACS

Dissociated cells were sorted based on EGFP fluorescence and gated such that only the top 2% brightest EGFP+ cells were collected for analysis for 30 and 48 hpf. Cells were sorted into 50 μ L 1xPBS/2% BSA in siliconized microcentrifuge tubes. Cell suspension was spun down at 350 x g at 4 °C for 5 min and the top 50 μ L was removed to enrich for viable cells.

Single cell RNA sequencing

EGFP+ cells from 50–100 dissociated embryos were used to create scRNA-seq libraries with Single Cell 3' v3 (10X Genomics) gene expression kits following manufacturer protocol. Samples were sequenced targeting ~50,000 reads per cell. Reads were aligned to GRCz11 using Cell Ranger version 3.1.0 (10X Genomics). Primary analysis was performed using Seurat v4⁹⁶. Data were filtered to retain cells with: 1,000–75,000 UMI counts, 1,900–9,000 unique genes expressed and <5% mitochondrial RNA. After quality control filtering the number of cells retained were: 1759 cells for 14 hpf; 10136 for 18 hpf dataset; 1378 for 22 hpf dataset; 9242 for two 30 hpf datasets; and 2107 for 48 hpf data set⁹⁷. All data sets, except one 30 hpf data set⁶³, were generated for this study. The pLL cluster was identified by expression of known lateral line markers but lack of marker expression of other cranial sensory neurons (*irx1a* and *phox2bb*) as well as anterior lateral line neurons (*alcama*). This cluster was then subjected to unsupervised subclustering, which yielded two distinct subpopulations, one of which was enriched for *ret*. Trajectory inference of pLL neurons from 14, 18, 22, 30, and 48 hpf was performed using Monocle3 with default parameters, with trajectory inference rooted (originating) at the pLL cell with the highest normalized *neurog1* expression.

Differential expression and gene signature analysis

To identify genes enriched in pioneer or follower pLL neuron subpopulations, differential expression (DE) analysis was performed with a minimum difference threshold set at 25% and FDR < 5% using the

'FindMarkers' function of Seurat. This analysis yielded 101 genes: 60 expressed in pioneers, 41 in followers. Genes with an average \log_2 fold change > 0.7 and p -value below 1×10^{-5} were considered enriched (20 enriched pioneer genes, and 7 enriched follower genes).

The Seurat function AddModuleScore was used to create gene signatures for pioneers and followers. Each signature consisted of top 20 DE gene at 30 hpf (sorted by \log_2 fold change; Table S1). The range of expression for each signature was normalized from 0 to 1 in order to visualize both signatures on the same scale (Fig. 5M, N).

Fluorescent in situ hybridization (RNAscope®)

Embryos were fixed in BT-fix (4% paraformaldehyde, 0.15 mM CaCl_2 , 4% sucrose, 0.1 M PO_4 buffer, pH = 7.3) overnight at 4 °C. Fixative was removed by 3×5 min washes in 1x PBS/0.01% Tween, followed by dehydration in a methanol series. Samples were then stored at -20 °C until processing. The RNAscope® Multiplex Fluorescent Detection Kit v2 following the Gross-Thebing et al. 2014 protocol was used with several modifications. Methanol was removed and samples were rehydrated with 1x PBS - 0.01% Tween. The protease step was omitted for samples younger than 48 hpf. Samples were then incubated overnight at 40 °C in 1:50 diluted probes. Probes were recovered and samples were washed in 0.2X SSCT (0.2X SSC and 0.01% Tween). Samples were then incubated at 40 °C according to the protocol in Amp1-3 using 2 drops of solution. After amplification, 2 drops of HRP matching the probe channel were added and samples were again incubated at 40 °C. Opal dyes 405, 570, and 650 were used at 1:1000. Washes between Amp solutions, HRP solutions, and Opal dyes were conducted using 1 quick rinse and 2×15 min 0.2x SSCT rinses. HRP blocker was used between channels prior to conjugating new HRPs but omitted before antibody incubation.

Immunofluorescence

Fluorescent in situ hybridization was followed by immunostaining to enhance transgene fluorescence. Samples underwent postfixation in 4% PFA for 10 min at RT. Fixative was then removed and embryos were washed in PBST (1x PBS/0.1% Triton) 3×20 min and blocked with 2% goat serum for 1 h at room temperature. Primary antibody (anti-EGFP 1:1000 and anti-mCherry 1:1000) was added and samples were incubated overnight at 4 °C with agitation. The primary antibody was removed with 3×15 min washes with PBST and secondary antibody (goat anti-chick or anti-rat 1:1000) was added and incubated for 4 h at 4 °C with agitation. Secondary antibody was washed out the same way, and DAPI (1:10000) was added to the final wash for samples requiring DNA labeling.

Confocal microscopy

For live imaging, embryos were mounted in 1.5% low melting point agarose in embryo medium on a glass cover slip and submersed in embryo media containing 0.02% tricaine. To observe neurogenesis and axon extension, embryos were imaged beginning at 14 hpf at 5–8 min intervals. All live imaging was performed on an upright Fluoview3000 confocal microscope (Olympus) using a 40x NA = 1.25 silicon oil immersion lens. Images through the pLLg or axon terminals were acquired with sufficient depth to capture the entire structure and all labeled cells/growth cones present. For fixed imaging, embryos were mounted in 50% glycerol/1x PBS and imaged on an upright Fluoview3000 confocal microscope (Olympus) using a 60x NA = 1.4 oil immersion lens.

Two-photon ablation

The published two-photon axotomy protocol⁶⁵ was followed with adaptations for whole cell ablations. Embryos were mounted at ~22 hpf, at the onset of pLL axon extension, on the multiphoton Zeiss LSM980 NLO microscope. Small, circular ROIs were drawn within each EGFP+ neuron and ablation was conducted using 80% laser

intensity for 1 microsecond at 910 nm. A brief 10 frame timelapse was taken, spanning the ablation, for visual confirmation that cells were ablated. After ablation, embryos were placed on the FV3000 confocal microscope and recorded for timelapse imaging over a period of 5 to 10 h.

Plasmid construction

The following plasmids were used or generated for this study: *5kb-neurod1:ret51-mcherry*⁵, *5kb-neurod1:EGFP-CAAX*, *5kb-neurod1:caRAR-EGFP-CAAX*, *5kb-neurod1:dnRAR-EGFP-CAAX*, *hsp70l:EGFP-CAAX;en.sill*, *hsp70l:caRAR-EGFP-CAAX;en.sill*, and *hsp70l:dnRAR-EGFP-CAAX;en.sill* using the Tol2kit⁹⁸. Plasmids containing middle entry dnRAR and caRAR were generously provided by the Waxman and Moens labs^{43,99}. Final constructs contained a 5' *5kb-neurod1* promoter¹⁰⁰ or a 3' *sill* enhancer¹⁰¹. Plasmids were purified using Qiagen column purification. Five to ten picograms of DNA constructs were injected into embryo cytoplasm at the 1- or 2-cell stage.

Creation of transgenic zebrafish lines

Tg(rpz5:mRuby)^{nl27} was created by knocking-in *mRuby* into the *rpz5* locus using a previously published mBait knock-in strategy¹⁰². Briefly, dualTRE *mBait-hsp70:mRuby* plasmid was injected into fertilized embryos together with the gRNA/Cas9 RNPs. gRNA targeted the start site at the *rpz5* locus: AGCGGTGTTTATGACTTCCG. The mBait-mRuby3 construct was a gift from the Raible lab which modified the original Shin-Ichi Higashijima's mBait-GFP construct. They generated the mBait-mRuby3 construct via Gibson assembly (Gibson et al., 2009), replacing the GFP protein sequence for the coding sequence of mRuby3. Following injections, fish were raised to adulthood and screened for transgene integration via fluorescence. Positive F1 progeny were validated via FISH using probes against mRuby and the endogenous *rpz5* message (Fig. S4A).

Tg(neurod1:mCherry)^{nl28}, *Tg(neurod1:kaede)*^{nl29} and *Tg(hsp70l:mCherry, en.sill)*^{nl30} were created by injecting 5 picograms of each plasmid into fertilized embryos together with 35 picograms of codon-optimized transposase⁹⁸. Following injections, F0 fish were raised to adulthood and their progeny were screened for transgene integration via fluorescence. Positive F1 adults were outcrossed one additional time before performing experiments to minimize use of animals with multiple integrations.

Kaede photoconversion and mosaic analysis

Photoconversions were performed using 40x NA = 1.25 silicon oil lens. Once the target cell was identified, a 20x zoom was used to magnify a region within the cell. An approximately 1 μm circular ROI was created and the region was scanned 20x with the 405 nm laser at 10% laser power. We labeled one cell per embryo, imaging total of 13 embryos. For mosaic analysis, embryos were generated by injection of 5 picograms *neurod1:mcherry* plasmid at the one-cell stage. Embryos were sorted for 1-3 labeled pLL neurons. We imaged 7 embryos that contained 4 pioneers and 7 followers.

Hoxb5a CRISPR-mediated knock down

Three guides targeting exon 1 of *hoxb5a* were designed as described according to published studies^{64,102}. Five hundred picograms of this triplex was injected into *cldnB:memgfp* embryos at the one-cell stage. At 30 hpf, EGFP-positive embryos were either fixed and processed for FISH or dissociated for DNA extraction and sequencing to assess indel frequency. PCR amplified the region targeted by all three guides and was sequenced through Premium PCR Sequencing by Plasmidsaurus using Oxford Nanopore Technology with custom analysis and annotation. All guides were efficient in producing indels: guide 1, 73%; guide 2, 93%; guide 3, 82% (Fig. S9A). Based on this, the estimated biallelic knockdown frequency is ~99.32%.

Quantification of axon targeting

To mosaically label neurons, embryos were injected with 10 picograms of plasmid. They were then screened at 48 hpf to identify embryos with 1–2 fluorescent cells. To track axon targeting, embryos were imaged between 48 and 72 hpf. Axons were followed from cell bodies and neuromast targets were recorded. Only embryos containing 1 to 2 neurons were used for the analysis, as additional labeled neurons impose greater difficulty in resolving single axon targets.

Quantification of fluorescent in situ hybridization

Confocal stacks of the pLLg were exported to Imaris (Bitplane) and analyzed using the Cells function. Neuron cell borders were constructed using the green channel from *cldnb:memgfp*. Accuracy of total cell numbers was achieved by counterstaining with DAPI such that every cell contained exactly one nucleus. The amplification from RNAscope® results in detectable individual mRNA transcripts, so fluorescent puncta were totaled in each cell. mRNA counts were separated into distinct bins from 0–10, with 10 as the maximum and 0 as the minimum observed in each embryo, for standardization across embryos.

SU5402 drug treatment

Embryos were incubated in 75 μ M SU5402 in 1% DMSO between 14–18 or 14–20 hpf. Following incubation, embryos were fixed in 4% PFA in 1x PBS and processed for in situ hybridization as described above.

Statistical analysis

Statistics were performed in either GraphPad or in R-Studio. Kendall Tau beta correlation coefficient was used to compare pairwise expression of candidate genes by FISH. When comparing expression of *ret* and *hoxb5a* after overexpression of RAR constructs, Kruskal-Wallis test with Dunn's multiple comparisons was used as the data were nonparametric. Mann-Whitney test was used for single comparisons between two groups of nonparametric data.

Reporting summary

Further information on research design is available in the Nature Portfolio Reporting Summary linked to this article.

Data availability

The scRNAseq datasets generated for this study have been deposited in the Gene Expression Omnibus (GEO) database under accession codes [GSE266312](#) and [GSE264323](#). One 30 hpf scRNA-seq dataset has been published previously and is available under accession code [GSE240721](#)⁶³. Source data are provided with this paper.

Code availability

R-code used in this study is available on GitHub: https://github.com/anechipor/Nechiporuk-lab-Woodruff_et_al_2024.

References

- Bate, C. M. Pioneer neurones in an insect embryo. *Nature* **260**, 54–56 (1976).
- Ho, R. K. & Goodman, C. S. Peripheral pathways are pioneered by an array of central and peripheral neurones in grasshopper embryos. *Nature* **297**, 404–406 (1982).
- Sánchez-Soriano, N. & Prokop, A. The influence of pioneer neurons on a growing motor nerve in drosophila requires the neural cell adhesion molecule homolog fasciclinII. *J. Neurosci.* **25**, 78–87 (2005).
- Lin, D. M., Auld, V. J. & Goodman, C. S. Targeted neuronal cell ablation in the Drosophila embryo: pathfinding by follower growth cones in the absence of pioneers. *Neuron* **14**, 707–715 (1995).
- Tuttle, A., Drerup, C. M., Marra, M., McGraw, H. & Nechiporuk, A. V. Retrograde Ret signaling controls sensory pioneer axon outgrowth. *eLife* **8**, e46092 (2019).
- Patel, C. K., Rodriguez, L. C. & Kuwada, J. Y. Axonal outgrowth within the abnormal scaffold of brain tracts in a zebrafish mutant. *J. Neurobiol.* **25**, 345–360 (1994).
- Chitnis, A. B. & Kuwada, J. Y. Elimination of a brain tract increases errors in pathfinding by follower growth cones in the zebrafish embryo. *Neuron* **7**, 277–285 (1991).
- Pike, S. H., Melancon, E. F. & Eisen, J. S. Pathfinding by zebrafish motoneurons in the absence of normal pioneer axons. *Development* **114**, 825–831 (1992).
- Gompel, N., Dambly-Chaudière, C. & Ghysen, A. Neuronal differences prefigure somatotopy in the zebrafish lateral line. *Development* **128**, 387–393 (2001).
- Liao, J. C. & Haehnel, M. Physiology of afferent neurons in larval zebrafish provides a functional framework for lateral line somatotopy. *J. Neurophysiol.* **107**, 2615–2623 (2012).
- Pujol-Martí, J., Baudoin, J.-P., Faucherre, A., Kawakami, K. & López-Schier, H. Progressive neurogenesis defines lateralis somatotopy. *Dev. Dyn.* **239**, 1919–1930 (2010).
- Sato, A., Koshida, S. & Takeda, H. Single-cell analysis of somatotopic map formation in the zebrafish lateral line system. *Dev. Dyn.* **239**, 2058–2065 (2010).
- Kulkarni, R. P., Bak-Maier, M. & Fraser, S. E. Differences in protein mobility between pioneer versus follower growth cones. *Proc. Natl. Acad. Sci. USA* **104**, 1207–1212 (2007).
- Nichols, E. L. & Smith, C. J. Pioneer axons employ Cajal's battering ram to enter the spinal cord. *Nat. Commun.* **10**, 562 (2019).
- Rapti, G. Regulation of axon pathfinding by astroglia across genetic model organisms. *Front. Cell. Neurosci.* **17**, 1241957 (2023).
- Rapti, G., Li, C., Shan, A., Lu, Y. & Shaham, S. Glia initiate brain assembly through noncanonical Chimaerin–Furin axon guidance in *C. elegans*. *Nat. Neurosci.* **20**, 1350–1360 (2017).
- Karkali, K., Vernon, S. W., Baines, R. A., Panayotou, G. & Martin-Blanco, E. Puckered and JNK signaling in pioneer neurons coordinates the motor activity of the Drosophila embryo. *Nat. Commun.* **14**, 8186 (2023).
- Chitnis, A. B., Dalle Nogare, D. & Matsuda, M. Building the posterior lateral line system in zebrafish. *Dev. Neurobiol.* **72**, 234–255 (2012).
- Ghysen, A. & Dambly-Chaudière, C. Development of the zebrafish lateral line. *Curr. Opin. Neurobiol.* **14**, 67–73 (2004).
- Piotrowski, T. & Baker, C. V. H. The development of lateral line placodes: Taking a broader view. *Dev. Biol.* **389**, 68–81 (2014).
- McGraw, H. F., Drerup, C. M., Nicolson, T. & Nechiporuk, A. V. The molecular and cellular mechanisms of zebrafish lateral line development. In *Auditory Development and Plasticity: Honor of Edwin W Rubel* (eds. Cramer, K. S., Coffin, A. B., Fay, R. R. & Popper, A. N.) 218 (Springer International Publishing, Cham, 2017).
- Kimmel, C. B., Ballard, W. W., Kimmel, S. R., Ullmann, B. & Schilling, T. F. Stages of embryonic development of the zebrafish. *Dev. Dyn.* **203**, 253–310 (1995).
- Gilmour, D., Knaut, H., Maischein, H.-M. & Nüsslein-Volhard, C. Towing of sensory axons by their migrating target cells in vivo. *Nat. Neurosci.* **7**, 491–492 (2004).
- Faucherre, A., Pujol-Martí, J., Kawakami, K. & López-Schier, H. Afferent neurons of the zebrafish lateral line are strict selectors of hair-cell orientation. *PLoS ONE* **4**, e4477 (2009).
- Nagiel, A., Andor-Ardó, D. & Hudspeth, A. J. Specificity of Afferent synapses onto plane-polarized hair cells in the posterior lateral line of the zebrafish. *J. Neurosci.* **28**, 8442–8453 (2008).
- Gompel, N. et al. Pattern formation in the lateral line of zebrafish. *Mech. Dev.* **105**, 69–77 (2001).

27. Alexandre, D. & Ghysen, A. Somatotopy of the lateral line projection in larval zebrafish. *Proc. Natl. Acad. Sci. USA* **96**, 7558–7562 (1999).
28. Obholzer, N. et al. Vesicular glutamate transporter 3 is required for synaptic transmission in zebrafish hair cells. *J. Neurosci.* **28**, 2110–2118 (2008).
29. Haas, P. & Gilmour, D. Chemokine signaling mediates self-organizing tissue migration in the zebrafish lateral line. *Dev. Cell* **10**, 673–680 (2006).
30. Andermann, P., Ungos, J. & Raible, D. W. Neurogenin1 defines zebrafish cranial sensory ganglia precursors. *Dev. Biol.* **251**, 45–58 (2002).
31. Mizoguchi, T., Togawa, S., Kawakami, K. & Itoh, M. Neuron and sensory epithelial cell fate is sequentially determined by notch signaling in zebrafish lateral line development. *J. Neurosci.* **31**, 15522–15530 (2011).
32. Nikaido, M., Navajas Acedo, J., Hatta, K. & Piotrowski, T. Retinoic acid is required and Fgf, Wnt, and Bmp signaling inhibit posterior lateral line placode induction in zebrafish. *Dev. Biol.* **431**, 215–225 (2017).
33. Albalat, R. & Cañestro, C. Identification of Aldh1a, Cyp26 and RAR orthologs in protostomes pushes back the retinoic acid genetic machinery in evolutionary time to the bilaterian ancestor. *Chem.-Biol. Interact.* **178**, 188–196 (2009).
34. Li, H. et al. Genetic contribution of retinoid-related genes to neural tube defects. *Hum. Mutat.* **39**, 550–562 (2018).
35. Thaller, C. & Eichele, G. Identification and spatial distribution of retinoids in the developing chick limb bud. *Nature* **327**, 625–628 (1987).
36. Durston, A. J. et al. Retinoic acid causes an anteroposterior transformation in the developing central nervous system. *Nature* **340**, 140–144 (1989).
37. Horton, C. & Maden, M. Endogenous distribution of retinoids during normal development and teratogenesis in the mouse embryo. *Dev. Dyn.* **202**, 312–323 (1995).
38. Costaridis, P., Horton, C., Zeitlinger, J., Holder, N. & Maden, M. Endogenous retinoids in the zebrafish embryo and adult. *Dev. Dyn.* **205**, 41–51 (1996).
39. Ghyselinck, N. B. et al. Role of the retinoic acid receptor beta (RARbeta) during mouse development. *Int. J. Dev. Biol.* **41**, 425–447 (1997).
40. Lohnes, D. et al. Function of the retinoic acid receptors (RARs) during development (I). Craniofacial and skeletal abnormalities in RAR double mutants. *Development* **120**, 2723–2748 (1994).
41. Rhinn, M. & Dollé, P. Retinoic acid signalling during development. *Development* **139**, 843–858 (2012).
42. Pennimpede, T. et al. The role of CYP26 enzymes in defining appropriate retinoic acid exposure during embryogenesis. *Birth Defects Res. Part A: Clin. Mol. Teratol.* **88**, 883–894 (2010).
43. Isabella, A. J., Barsh, G. R., Stonick, J. A., Dubrulle, J. & Moens, C. B. Retinoic acid organizes the zebrafish vagus motor topographic map via spatiotemporal coordination of Hgf/Met signaling. *Dev. Cell* **53**, 344–357.e5 (2020).
44. Liu, R.-Z. et al. Retention of the duplicated cellular retinoic acid-binding protein 1 genes (crabp1a and crabp1b) in the zebrafish genome by subfunctionalization of tissue-specific expression. *FEBS J.* **272**, 3561–3571 (2005).
45. Oosterveen, T. et al. Retinoids regulate the anterior expression boundaries of 5' Hoxb genes in posterior hindbrain. *EMBO J.* **22**, 262–269 (2003).
46. Mahony, S. et al. Ligand-dependent dynamics of retinoic acid receptor binding during early neurogenesis. *Genome Biol.* **12**, R2 (2011).
47. Kessel, M. Respecification of vertebral identities by retinoic acid. *Development* **115**, 487–501 (1992).
48. Kessel, M. & Gruss, P. Homeotic transformations of murine vertebrae and concomitant alteration of Hox codes induced by retinoic acid. *Cell* **67**, 89–104 (1991).
49. Waxman, J. S., Keegan, B. R., Roberts, R. W., Poss, K. D. & Yelon, D. Hoxb5b acts downstream of retinoic acid signaling in the forelimb field to restrict heart field potential in zebrafish. *Dev. Cell* **15**, 923–934 (2008).
50. Matsuda, H. & Kubota, Y. Zebrafish pancreatic β cell clusters undergo stepwise regeneration using Neurod1-expressing cells from different cell lineages. *Cell Tissue Res.* **394**, 131–144 (2023).
51. Burzynski, G. M., Delalande, J.-M. & Shepherd, I. Characterization of spatial and temporal expression pattern of SCG10 during zebrafish development. *Gene Expr. Patterns* **9**, 231–237 (2009).
52. Rentzsch, F., Zhang, J., Kramer, C., Sebald, W. & Hammerschmidt, M. Crossveinless 2 is an essential positive feedback regulator of Bmp signaling during zebrafish gastrulation. *Development* **133**, 801–811 (2006).
53. Wada, H., Dambly-Chaudière, C., Kawakami, K. & Ghysen, A. Innervation is required for sense organ development in the lateral line system of adult zebrafish. *Proc. Natl. Acad. Sci. USA* **110**, 5659–5664 (2013).
54. Cheng, C. W. et al. Zebrafish homologue irx1a is required for the differentiation of serotonergic neurons. *Dev. Dyn.* **236**, 2661–2667 (2007).
55. Nechiporuk, A., Linbo, T. & Raible, D. W. Endoderm-derived Fgf3 is necessary and sufficient for inducing neurogenesis in the epibranchial placodes in zebrafish. *Development* **132**, 3717–3730 (2005).
56. Wilson, A. L. et al. Cadherin-4 Plays a role in the development of zebrafish cranial ganglia and lateral line system. *Dev. Dyn.* **236**, 893–902 (2007).
57. Dupé, V. et al. In vivo functional analysis of the Hoxa-1 3' retinoic acid response element (3'RARE). *Development* **124**, 399–410 (1997).
58. Serpente, P. et al. Direct crossregulation between retinoic acid receptor β and Hox genes during hindbrain segmentation. *Development* **132**, 503–513 (2005).
59. Kruse, S. W. et al. Identification of COUP-TFII orphan nuclear receptor as a retinoic acid-activated receptor. *PLoS Biol.* **6**, e227 (2008).
60. Kim, T.-S. et al. The ZFX3 (ATBF1) transcription factor induces PDGFRB, which activates ATM in the cytoplasm to protect cerebellar neurons from oxidative stress. *Dis. Models Mech.* **3**, 752–762 (2010).
61. Wang, F. et al. RNAscope: A novel in situ RNA analysis platform for formalin-fixed, paraffin-embedded tissues. *J. Mol. Diagn.* **14**, 22–29 (2012).
62. Gross-Thebing, T., Paksa, A. & Raz, E. Simultaneous high-resolution detection of multiple transcripts combined with localization of proteins in whole-mount embryos. *BMC Biol.* **12**, 55 (2014).
63. Olson, H. M. et al. RhoA GEF Mcf2lb regulates rosette integrity during collective cell migration. *Development* **151**, dev201898 (2024).
64. Ota, S. et al. Functional visualization and disruption of targeted genes using CRISPR/Cas9-mediated eGFP reporter integration in zebrafish. *Sci. Rep.* **6**, 34991 (2016).
65. O'Brien, G. S. et al. Two-photon axotomy and time-lapse confocal imaging in live zebrafish embryos. *J. Vis. Exp. (JoVE)* **16**, 1129 (2009).
66. Bandla, A. et al. A new transgenic tool to study the ret signaling pathway in the enteric nervous system. *Int. J. Mol. Sci.* **23**, 15667 (2022).
67. Hidalgo, A. & Brand, A. H. Targeted neuronal ablation: the role of pioneer neurons in guidance and fasciculation in the CNS of Drosophila. *Development* **124**, 3253–3262 (1997).

68. Jin, S. et al. Inference and analysis of cell-cell communication using CellChat. *Nat. Commun.* **12**, 1088 (2021).
69. Schuster, K., Dambly-Chaudière, C. & Ghysen, A. Glial cell line-derived neurotrophic factor defines the path of developing and regenerating axons in the lateral line system of zebrafish. *Proc. Natl Acad. Sci. USA* **107**, 19531–19536 (2010).
70. Nittoli, V. et al. A comprehensive analysis of neurotrophins and neurotrophin tyrosine kinase receptors expression during development of zebrafish. *J. Comp. Neurol.* **526**, 1057–1072 (2018).
71. Pan, Y. A. et al. Zebrow: multispectral cell labeling for cell tracing and lineage analysis in zebrafish. *Development* **140**, 2835–2846 (2013).
72. Cook, Z. T. et al. Combining near-infrared fluorescence with Brainbow to visualize expression of specific genes within a multicolor context. *MBoC* **30**, 491–505 (2019).
73. Sarrazin, A. F. et al. Origin and early development of the posterior lateral line system of zebrafish. *J. Neurosci.* **30**, 8234–8244 (2010).
74. Metcalfe, W. K. Organization and development of the zebrafish posterior lateral line. In *The Mechanosensory Lateral Line* (eds. Coombs, S., Görner, P. & Münz, H.) 147–159 (Springer, New York, NY, 1989).
75. Becht, E. et al. Dimensionality reduction for visualizing single-cell data using UMAP. *Nat. Biotechnol.* **37**, 38–44 (2019).
76. Madelaine, R., Garric, L. & Blader, P. Partially redundant proneural function reveals the importance of timing during zebrafish olfactory neurogenesis. *Development* **138**, 4753–4762 (2011).
77. Bertrand, N., Castro, D. S. & Guillemot, F. Proneural genes and the specification of neural cell types. *Nat. Rev. Neurosci.* **3**, 517–530 (2002).
78. Washbourne, P. et al. Genetic ablation of the t-SNARE SNAP-25 distinguishes mechanisms of neuroexocytosis. *Nat. Neurosci.* **5**, 19–26 (2002).
79. Tafoya, L. C. R. et al. Expression and function of SNAP-25 as a universal SNARE component in GABAergic neurons. *J. Neurosci.* **26**, 7826–7838 (2006).
80. Ahmed, M., Xu, J. & Xu, P.-X. EYA1 and SIX1 drive the neuronal developmental program in cooperation with the SWI/SNF chromatin-remodeling complex and SOX2 in the mammalian inner ear. *Development* **139**, 1965–1977 (2012).
81. Trapnell, C. et al. The dynamics and regulators of cell fate decisions are revealed by pseudotemporal ordering of single cells. *Nat. Biotechnol.* **32**, 381–386 (2014).
82. del Corral, R. D. et al. Opposing FGF and Retinoid pathways control ventral neural pattern, neuronal differentiation, and segmentation during body axis extension. *Neuron* **40**, 65–79 (2003).
83. Martínez-Morales, P. L. et al. FGF and retinoic acid activity gradients control the timing of neural crest cell emigration in the trunk. *J. Cell Biol.* **194**, 489–503 (2011).
84. Deschamps, J. & van Nes, J. Developmental regulation of the Hox genes during axial morphogenesis in the mouse. *Development* **132**, 2931–2942 (2005).
85. Cunningham, T. J. & Ducrest, G. Mechanisms of retinoic acid signalling and its roles in organ and limb development. *Nat. Rev. Mol. Cell Biol.* **16**, 110–123 (2015).
86. Mohammadi, M. et al. Structures of the tyrosine kinase domain of fibroblast growth factor receptor in complex with inhibitors. *Science* **276**, 955–960 (1997).
87. Maroon, H. et al. Fgf3 and Fgf8 are required together for formation of the otic placode and vesicle. *Development* **129**, 2099–2108 (2002).
88. Schlosser, G. Induction and specification of cranial placodes. *Dev. Biol.* **294**, 303–351 (2006).
89. Begemann, G. & Meyer, A. Hindbrain patterning revisited: timing and effects of retinoic acid signalling. *BioEssays* **23**, 981–986 (2001).
90. Bleckmann, H. *Flow Sensing in Air and Water: Behavioral, Neural and Engineering Principles of Operation* 2014th edition, Vol. 562 (Springer, Berlin, Heidelberg, 2014).
91. Eisen, J. S., Myers, P. Z. & Westerfield, M. Pathway selection by growth cones of identified motoneurons in live zebra fish embryos. *Nature* **320**, 269–271 (1986).
92. Kuwada, J. Y. Cell recognition by neuronal growth cones in a simple vertebrate embryo. *Science* **233**, 740–746 (1986).
93. McConnell, S. K., Ghosh, A. & Shatz, C. J. Subplate neurons pioneer the first axon pathway from the cerebral cortex. *Science* **245**, 978–982 (1989).
94. Ghosh, A., Antonini, A., McConnell, S. K. & Shatz, C. J. Requirement for subplate neurons in the formation of thalamocortical connections. *Nature* **347**, 179–181 (1990).
95. Covassin, L. et al. Global analysis of hematopoietic and vascular endothelial gene expression by tissue specific microarray profiling in zebrafish. *Dev. Biol.* **299**, 551–562 (2006).
96. Hao, Y. et al. Integrated analysis of multimodal single-cell data. *Cell* **184**, 3573–3587.e29 (2021).
97. Satija, R., Farrell, J. A., Gennert, D., Schier, A. F. & Regev, A. Spatial reconstruction of single-cell gene expression. *Nat. Biotechnol.* **33**, 495–502 (2015).
98. Kwan, K. M. et al. The Tol2kit: a multisite gateway-based construction kit for Tol2 transposon transgenesis constructs. *Dev. Dyn.* **236**, 3088–3099 (2007).
99. Waxman, J. S. & Yelon, D. Zebrafish retinoic acid receptors function as context-dependent transcriptional activators. *Dev. Biol.* **352**, 128 (2011).
100. Mo, W. & Nicolson, T. Both pre- and postsynaptic activity of Nsf prevents degeneration of hair-cell synapses. *PLOS ONE* **6**, e27146 (2011).
101. Pujol-Martí, J. et al. Neuronal birth order identifies a dimorphic sensorineural map. *J. Neurosci.* **32**, 2976–2987 (2012).
102. Kimura, Y., Hisano, Y., Kawahara, A. & Higashijima, S. Efficient generation of knock-in transgenic zebrafish carrying reporter/driver genes by CRISPR/Cas9-mediated genome engineering. *Sci. Rep.* **4**, 6545 (2014).

Acknowledgements

The cell sorting for scRNA-seq was performed in the OHSU Flow Cytometry Shared Resource. This shared resource is supported, in part, by the OHSU Knight Cancer Institute NCI Cancer Center Support Grant P30CA069533. We also acknowledge expert assistance from staff of the OHSU Advanced Light Microscopy Core (RRID:SCR_009961). Short read sequencing assays were performed by the OHSU Massively Parallel Sequencing Shared Resource. Figure schematics were generated in BioRender Lab, N. (2025) <https://BioRender.com/y61d490>. We thank Drs. Joshua Waxman, Cecilia Moens, David Raible, and Julia Ganz for providing reagents. We are also grateful to Dr. Adam Miller for stimulating discussions at the onset of this study. Finally, we thank Drs. Kevin Wright, Kelly Monk, John Brigande, and Philip Copenhagen for their comments on the manuscript. N.L.C. acknowledges funding from the NCI/NIH under award number T32CA254888. The study was funded by NIH awards, NS111419 and NS112795 to A.V.N.

Author contributions

B.M.W. and A.V.N. conceptualized the project. BMW performed the majority of experiments in the study. L.M.N. performed the initial set of scRNA-seq experiments. N.L.C. and L.M.H. performed initial scRNA-seq data analysis. A.V.N., L.N.M., and B.M.W. performed subsequent analysis. A.V.N. and JRM performed imaging, drug treatment, and CRISPR knockdown experiments. B.M.W. performed all Imaris image analysis. A.V.N. and L.M.H. supervised the project. BMW authored the text and prepared the manuscript with editing from A.V.N. as well as all other contributors.

Competing interests

The authors declare no competing interests.

Inclusion & ethics statement

This research aligns with the Inclusion & ethical guidelines embraced by Nature Communications.

Additional information

Supplementary information The online version contains supplementary material available at

<https://doi.org/10.1038/s41467-025-61044-1>.

Correspondence and requests for materials should be addressed to Alex V. Nechiporuk.

Peer review information *Nature Communications* thanks Berta Alsina and the other, anonymous, reviewer(s) for their contribution to the peer review of this work. A peer review file is available.

Reprints and permissions information is available at <http://www.nature.com/reprints>

Publisher's note Springer Nature remains neutral with regard to jurisdictional claims in published maps and institutional affiliations.

Open Access This article is licensed under a Creative Commons Attribution-NonCommercial-NoDerivatives 4.0 International License, which permits any non-commercial use, sharing, distribution and reproduction in any medium or format, as long as you give appropriate credit to the original author(s) and the source, provide a link to the Creative Commons licence, and indicate if you modified the licensed material. You do not have permission under this licence to share adapted material derived from this article or parts of it. The images or other third party material in this article are included in the article's Creative Commons licence, unless indicated otherwise in a credit line to the material. If material is not included in the article's Creative Commons licence and your intended use is not permitted by statutory regulation or exceeds the permitted use, you will need to obtain permission directly from the copyright holder. To view a copy of this licence, visit <http://creativecommons.org/licenses/by-nc-nd/4.0/>.

© The Author(s) 2025